



Full Length Article

脉冲宽度和频率

Influence of pulse duration and pulse frequency on micro-roughness for laser micro polishing (L μ P) of stainless steel AISI 410A. Temmler^{a,c,*}, D. Liu^a, J. Luo^a, R. Poprawe^{a,b,c}^a State Key Laboratory of Tribology, Tsinghua University, 100084 Beijing, PR China^b Fraunhofer Institute for Lasertechnology, 52074 Aachen, Germany^c Chair for Lasertechnology, RWTH Aachen University, 52074 Aachen, Germany

ARTICLE INFO

Keywords:

Laser polishing
AISI410
Surface roughness
Remelting
High pressure laminates
Press plates

ABSTRACT

装饰薄层的压板

Press plates for decorative laminates are often made from AISI410 and typically need a surface finish created by polishing. A new manufacturing process that can overcome disadvantages from conventional polishing processes is laser micro-polishing (L μ P). Therefore, this experimental investigation focuses on the effect of L μ P on the micro-roughness in the nanometer range for stainless steel AISI410. This study closes a gap regarding investigations for L μ P with pulse durations from 10 ns to 220 ns and pulse frequencies from 20 kHz to 240 kHz using a commercially available 35 W fiber laser. The feasibility for L μ P on AISI410 in terms of achieved micro-roughness and avoidance of surface defects was successfully demonstrated. A significant reduction of surface roughness was achieved using pulse durations as short as 10 ns and pulse frequencies as high as 240 kHz. In addition, indications for a fundamental change of the process from a discrete, pulsed process to a continuous remelting process were observed and an empirical estimation for the prediction of this change was derived. Furthermore, spatially resolved laser polishing was demonstrated on textured press plates. With area rates of up to several square meters per hour within reach, L μ P on AISI410 stands ready for industrial implementation.

AISI 410的面积率高达每小时数平方米, 可用于工业应用

1. Introduction

The surface of a component increasingly determines its function and often has a significant influence on the subsequent appearance of the overall product. Therefore, the production of a required surface represents an important step in industrial manufacturing processes. A surface finishing step used in many areas of industrial production is polishing. Polishing processes are typically carried out abrasively, i.e. by areal and/or local removal of material. This material removal makes it particularly difficult to maintain surface geometries such as sharp edges. In addition, polishing of three-dimensional freeform surfaces is a challenging task, which up to now often had to be performed manually and in a very time-consuming manner. The achievable surface quality depends strongly on the material, its quality, the complexity of the components geometry, and the capabilities of the manual polisher. On the one hand, this can lead to inhomogeneous roughness over the entire component (if this can be tested at all, since accessibility for a corresponding topography measurement is not necessarily given). On the other hand, this can lead to limited reproducibility from component to component. In addition, manual polishing processes are often very cost-intensive, as the corresponding time expenditure and personnel costs are high, especially

in high-wage countries. This limited extent of automation makes manual polishing less attractive for manufacturers in light of future challenges. Finally, selective polishing of surface areas smaller than a few square millimeters (for example on textured press plates for high-pressure decorative laminates) is another technical challenge that is difficult to master with conventional polishing techniques.

In the course of the last 15 years, substantial experimental and theoretical studies on laser micro polishing (L μ P) of metals have been carried out. Bordatchev et al. [1] provide an extensive overview of laser polishing performance for metals. Until now, the feasibility of L μ P has been successfully demonstrated on a variety of metals ranging from tool and stainless steels to nickel and titanium alloys. Nüsser [2] has compiled a detailed overview of laser micro polishing results for different materials, which are systematically evaluated and listed according to the most important process parameters. In general, the applicability of laser polishing has widened from the early mold and die/laser-sintered components into aerospace and biomedical sectors. The automatable, contactless processing without mechanical tool wear, the elimination of grinding and polishing agents, the avoidance of intermediate cleaning steps, removal residues and material loss, the excellent geometric accuracy, the high processing speeds, the high reproducibility and the

* Corresponding author at: State Key Laboratory of Tribology, Tsinghua University, 100084 Beijing, PR China.

E-mail addresses: atemmler@tsinghua.edu.cn, andre.temmler@rwth-aachen.de (A. Temmler).

high chemical cleanliness of the surfaces are essential advantages of L μ P compared to conventional polishing processes. Furthermore, L μ P can not only be used for areal laser polishing but also enables polishing with high spatial resolution, so that only selected parts of a surface can be laser polished without affecting the rest of the surface. Additionally, since no material is removed, no environmental contamination occurs during L μ P.

For L μ P, usually single-step or sometimes multi-step laser polishing processes on flat samples or free-form surfaces are used. Multi-step laser polishing processes have been introduced, especially by Willenborg [3] in his groundbreaking work on laser polishing of metals with continuous and pulsed laser radiation. Temmler [4] demonstrated further that a multi-step process (subsequent polishing with continuous and pulsed laser radiation) leads to a significant reduction in roughness of a metallic surface (AISI H11) for areal and selective laser polishing. In these cases, an effective smoothing of the roughness was achieved with a combination of laser macro polishing and L μ P. L μ P was used to smooth the micro-roughness, especially in the nanometer range, and thus significantly increased the gloss level of a surface. Pfefferkorn et al. [5] used a dual-step L μ P process to smooth surface roughness. In the first step, process parameters were selected in such a way that an assumed Marangoni flow occurred. This resulted in wavy surfaces due to material accumulation at the edges of the remelted zones for each individual laser spot. To eliminate the induced waviness the surface was then laser polished a second time, whereby the laser beam diameter and laser power were selected in such a way that no material accumulation occurred anymore. For a single-step laser polishing process, Nüsser [2] demonstrated that area rates of up to 8.8 min/m² are feasible. Furthermore, Temmler [6] demonstrated the feasibility of L μ P for an actual three-dimensional free-form surface. They reported that the complex surface of a left ventricular assisting device for a cardiac support system could be polished entirely by L μ P. While the processing time for conventional manual polishing is approx. 3.5 h, approx. 10 min were required for L μ P including non-productive times, which resulted in an area rate of approx. 37 s/cm². A first version of a complete CAD-CAM data chain for an automated laser polishing of free-form surfaces was developed by Ostholt [7]. This first version was overhauled, enhanced and significantly extended by Flemmer [8]. The current version of this CAD-CAM data and process chain is now available for path planning and laser polishing of complex shaped parts utilizing 5 + 3 axes machining or even 9-axis simultaneous machining. Although a complete data chain for laser polishing of 3D parts has been fully developed and its feasibility has been demonstrated multiple times, laser polishing still struggles to make the decisive step into widespread industrial application. Besides smaller technical challenges, there is also a lack of basic understanding of the polishing/remelting process and its interaction with the material. This results in surface roughness that is often not sufficiently smooth for an aimed application. Outstanding results were reported by Temmler et al. [6] with a minimal surface roughness of Ra = 0.08 μ m for laser micro-polished Ti6Al4V components. In addition, Kiedrowski [9] achieved a minimal roughness of Ra = 0.05 μ m on tool steel AISI H11. However, in general, laser polishing struggles to achieve high gloss surface polishing. An additional major challenge is the wide variety of different materials and material qualities used in industrial production.

To increase the understanding of the laser polishing process, modelling of L μ P of metals was introduced by Shao et al. [10]. Based on an analysis of heat transfer and taking evaporation of surface asperities into account, Shao et al. [10] identified that the melt duration of a surface is of crucial significance for L μ P. Perry [11] deepened that understanding significantly and developed a model for estimating the spectral composition of surface roughness after L μ P¹. Based on the assumption that the amplitudes of molten asperities decay sinusoidally

¹ It should be noted that this model is only valid without further restrictions if there is no material flow in the melt pool (e.g. Marangoni flow).

under the influence of viscosity and surface tension, the surface geometry was modeled before and after laser polishing. Perry [11] defined a decay time t for capillary waves. Amplitudes of the spatial frequencies are smoothed where the melt duration of the melt pool is significantly longer than the decay time of the spatial frequency. Furthermore, the smaller the spatial frequency, the longer the decay time, so that the so-called critical spatial frequency f_{cr} was defined by Perry [11] for a constant melt duration of the melt pool. Spatial frequencies that are significantly higher than this critical spatial frequency are almost completely smoothed. Spatial frequencies that are significantly lower than the critical spatial frequency remain largely unaffected². The critical spatial frequency depends on the density ρ and the dynamic viscosity η of the material as well as on the melt duration t_M and can be estimated by Eq. (3.1).

$$f_{cr} = \sqrt{\frac{\rho}{8\pi^2 \cdot \eta \cdot t_M}} \quad (3.1)$$

This model was validated by means of experimental investigations. Although the results showed quantitative deviations, a qualitative agreement between numerical simulation and experimental results has already been achieved by Perry [11]. Analogously, Chow et al. [12] find that L μ P is a 1st order low-pass filter that is applied onto the initial surface and results in a smoothed surface (if process parameters are chosen correctly). The model developed by Perry [11] was further enhanced and extended by Vadali et al. [13] so that roughness of the laser micro-polished surface can be calculated from a line profile of the original surface. Their experimental investigations showed an accuracy of up to 90%. Vadali et al. [14] extended the model to three-dimensional surface topographies and thus to a two-dimensional, Gauss weighted low-pass filter. This resulted in an accuracy of up to 99.5 percent for modeling of surface roughness after L μ P using selected process parameters on the material Ti6Al4V³.

However, although the international scientific laser polishing community largely agrees that longer melt durations lead to a reduced surface roughness, some controversy still arises from the question of whether Marangoni flow is a significant mechanism in L μ P. Besides surface smoothing due to L μ P, Vadali et al. [15] observed a border bulging in the size of the laser spot at the edge of each individual remelting area. This border bulging resulted in a wavy surface. Laser polishing and border bulging were attributed to the fact that Marangoni flow occurred in the melt pool. Marangoni flow was assumed to have a positive effect on the smoothing of the roughness of long spatial wavelengths, but is also assumed to lead to border bulging. According to Ma et al. [16], the occurrence of Marangoni flow depends, among other things, on the laser beam diameter. Ma et al. [17] developed a model with which the deformation of the melt pool surface due to the Marangoni flow and the remelting depth could be determined. Ma et al. [17] assumed further that the occurrence of a Marangoni flow during L μ P depends significantly on the process parameters. The probability of occurrence seems to increase with longer pulse duration, smaller laser

² For a specific material, the critical spatial frequency depends only on melt duration t_M , which is essentially determined by pulse energy, laser beam dimensions and pulse duration. The longest possible melt duration t_M was estimated on the basis of the highest intensity (which led to a remelting, but not to a material removal by evaporation) using heat conduction simulation. On the basis of this melt duration t_M , the lowest possible critical spatial frequency was calculated. The effect of a possible heat accumulation is not considered in the model.

³ Vadali et al. [15] showed that their model for L μ P of TiAl6V4 with pulse durations of $t_p = 1.91 \mu$ s and $t_p = 3.60 \mu$ s is no longer valid and the roughness achieved by L μ P is only 52% ($t_p = 1.91 \mu$ s) or 60% ($t_p = 3.60 \mu$ s) of the calculated roughness, i.e. the roughness is more effectively reduced than calculated. These results are in contrast to the described results for L μ P of Ti6Al4V and SS316L with a pulse duration of $t_p = 5.0 \mu$ s in [13], where the accuracy of the roughness calculation is 90%.

beam diameter and higher fluence.

In contradiction to this assumption, Nüsser et al. [18] hypothesized that border bulges are presumably not a result of Marangoni flow. They stated that the time necessary for the formation of Marangoni flow in melt pools during laser remelting processes is in the range of milliseconds. Since the pulse duration is several microseconds, this time is much shorter than needed to generate a Marangoni flow. Furthermore, Nüsser [2] stated that the reason for border bulging is partial material ablation that leads to a considerable vapor pressure or recoil pressure above the melt pool. This recoil pressure leads to a deformation of the melt pool surface and surface structures. Nüsser [2] explicitly pointed out that a Marangoni flow is very unlikely to be responsible for this kind of material redistribution. In addition to his own investigations, Nüsser [2] relies above all on the investigations of Cho et al. [19] for the numerical analysis of melt pool oscillations during laser welding. This analysis has shown that vapor pressure above the weld pool has a significant influence on the surface topography, while the influence of Marangoni convection is negligibly small in comparison. In addition, Temmler et al. [20] demonstrated that surface structuring can be achieved with localized vaporization of small amounts of molten material from a melt pool. Localized vaporization presumably creates vapor or recoil pressure that leads to a deformation of the melt pool surface in the form of capillary surface waves [21]. These deformations of the melt pool surface then subsequently resolidify in the deformed state and lead to formation of surface structures.

With regard to this controversy about the influence of a possible Marangoni convection on the smoothing behavior of L μ P, the investigations of comparatively high pulse frequencies (up to 240 kHz) are of particular interest. As soon as the time interval of successive pulses is shorter than the existence time of the melt pool, there is no longer a discrete remelting process. In this case, the discrete remelting process would change to a quasi-continuous remelting process with fundamentally different characteristics and smoothing behavior. The melting time would reach an order of magnitude that would no longer exclude the possibility of Marangoni convection. Whether indications of such a quasi-continuous laser polishing process can be observed in the context of these investigations could therefore be of significant relevance for a fundamentally deeper understanding of the laser polishing process.

1.1. Aims and novelty of this investigation

Examination of the published theoretical and experimental studies on laser micro polishing shows a considerable need for further research and development. One need arises especially from the wide variety of different materials that are often used for specific applications. Previous studies showed that results for laser micro polishing strongly depend on the material. Therefore, for each material or even for different qualities of the same material, the suitability of the specific materials must be explicitly tested. In this study, the feasibility of L μ P for stainless steel AISI 410 is investigated systematically. AISI 410 is often used for press plates of decorative laminates. Therefore, the main foci of this investigation lie on the evaluation of micro-roughness and the avoidance of surface defects such as holes, cracks or scratches. In terms of ensuring industrial applicability, a commercially available fiber laser system within a comparatively simple optical set-up and a wide range of adaptable process parameters are used. Furthermore, an evaluation of feasibility for industrial application in terms of achievable area rates will be given. The feasibility of selective laser polishing will be demonstrated on selected, textured press plates.

In order to achieve these overarching, application-oriented aims, fundamental investigations are carried out on the influence of pulse duration (in the range of $t_p = 10$ ns to 220 ns) and pulse frequency (in the range of $f_p = 20$ kHz to 240 kHz) on surface roughness. This range of process parameters is typical for commercially available fiber lasers and has not been investigated yet. Based on these investigations,

correlations between process parameters and achieved surface roughness will be identified. This applies in particular to the influence of fluence, temporal pulse-pulse distance, number of remeltings, or the basic characteristics of the remelting process (discrete or continuous) on the micro-roughness of a surface. With the exception of fluence, the influence of these process parameters on roughness have only been investigated marginally in other studies.

Therefore, key novelties of this investigation are the following:

1. Investigation of feasibility of stainless steel AISI 410 for laser micro polishing
2. Systematic investigation on the influence of selected process parameters on micro-roughness after L μ P:
 - (a) Pulse durations from $t_p = 10$ ns to $t_p = 220$ ns
 - (b) Repetition frequencies from $f_p = 20$ kHz to $f_p = 240$ kHz
 - (c) Number of remelting cycles from $n = 7.2$ to $n = 85.8$
3. Deriving an empirical formula for a change of the remelting process from a discrete, pulsed L μ P process to a continuous remelting process
4. Demonstration of feasibility for selective laser polishing of textured press plates (for decorative laminates) made from AISI 410

2. Experimental

2.1. Process principle

A new manufacturing process for surface finishing is laser micro polishing (L μ P) with pulsed laser radiation. L μ P is based on the local redistribution of material in the liquid phase and not, as in conventional polishing processes, on the removal of material. L μ P is a complex thermodynamic process involving initial surface topography, thermal time-dependent material properties, a variety of adjustable process parameters, and the interaction between laser radiation and metals as well as their individual thermal phenomena. In general, L μ P with pulsed laser radiation is a combination of remelting and evaporation of micro asperities. The mechanism dominating the L μ P process is the flowing of molten material of a thin surface layer under the effect of surface tension. A remelting depth of less than five micrometers is usually achieved, which specifically reduces the micro-roughness, i.e. roughness with low spatial wavelengths (< 40 μ m) and amplitudes (< 100 nm). In particular, the gloss of a surface is increased by L μ P, while the waviness of the surface remains almost unaffected. Thus, L μ P is dominated by the remelting of a very thin surface layer and has only a small influence on conventionally measured roughness values such as Ra and Rz.

Due to the process parameters typically used, i.e. pulse duration of several hundred nanoseconds, repetition frequencies up to several tens of kilohertz, scanning velocities usually larger than 100 mm/s and laser beam diameters in the range of micrometers, the molten material is already resolidified before a subsequent laser pulse creates another melt pool (Fig. 1). Temmler [4] thus states that L μ P is typically a discontinuous, discrete process rather than a continuous remelting process. Investigations described in the literature frequently use laser beam diameters in the range of 30–300 μ m⁴. Therefore, due to the high ratio of laser beam diameter to remelting depth, Willenberg [3] assumes a one-dimensional heat conduction state during L μ P.

⁴ An exception to this is the investigation of Bordatchev et al. [22] who uses pulse durations in the picosecond range ($t_p = 10.5$ ps) with a pulse frequency in the megahertz range ($f_p = 7.45$ MHz). Chen et al. [23] also use a pulse frequency of $f_p = 10$ MHz for laser polishing with picosecond laser pulses ($t_p = 10$ ps). However, this is a feasible way to prolong the melt duration due to local heat accumulation of a surface and might more likely be a continuous than a discrete laser remelting process.

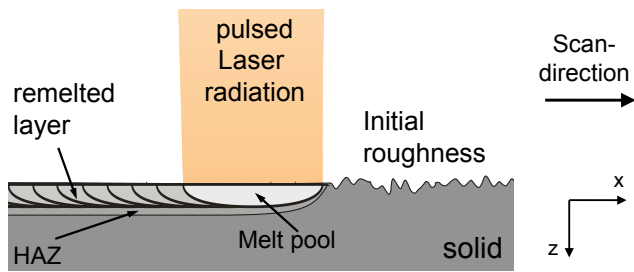


Fig. 1. Schematic of laser polishing by remelting a thin surface layer with pulsed laser radiation [35].

2.1.1. Areal laser polishing

Willenborg [3] presents a common and widespread scanning strategy for surfaces using meandering processing. For $L_{\mu}P$ of a surface, the circular laser beam is moved in a meandering pattern over the surface to be polished (Fig. 2).

After each scan vector, the laser beam is offset in parallel by the track offset dy , which is usually significantly smaller than the width of the remelted track. For $L_{\mu}P$ this corresponds approximately to the laser beam diameter. Vadali [24] found that due to the discontinuous process, the orientation of the machining pattern relative to the workpiece surface has in principle no effect on the achievable roughness. Furthermore, Nüsser [2] comes to the conclusion that the orientation of the main scan direction relative to structures of the initial roughness as well as the orientation of a square laser beam focus relative to the main scan direction have no influence on the resulting roughness. However, Morrow [25] found a significant decrease in local hardness for overlapping areal polishing due to complex back-tempering cycles of subsequent laser pulses and laser tracks.

Chow et al. [12] identify four major categories of process parameters that play a significant role in $L_{\mu}P$. These four categories are workpiece-, laser-, optics- and motion-related process parameters. In practice, however, the individual process parameters are not only assigned to one category but to several. For example, the laser beam diameter is based both on the properties of the laser beam source and on those of the optical set-up. In this context, important process parameters for $L_{\mu}P$ that mainly result from the characteristics of laser beam source and optical set-up are maximum laser power, pulse repetition rate (PRR), pulse duration, pulse shape, maximum pulse energy, beam quality, intensity distribution, laser beam diameter and Rayleigh-length. Concerning the strategy of laser processing, noticeable parameters are average laser power, laser beam diameter d_L , scanning

velocity v_{scan} , pulse repetition rate (PRR) f_p , scan length, track offset dy , inclination angle β , number of repetitions n , and focal offset dz .

Track width w_{track} , micro-structure, and resulting surface roughness (Ra, Sa, Sa-spectrum) for example are also significantly influenced by the material that is laser polished. This category also includes all properties of the remelted surface layer, such as hardness, residual stress, corrosion resistance, adhesion, etc.

2.1.2. Selective laser polishing

Selective laser polishing is a special method of laser polishing in which a surface is only partially remelted and selected areas are smoothed with high spatial resolution. This method was investigated fundamentally and presented in detail by Temmler et al. [26]. Based on these results, Temmler [4] developed a complete process chain for selective laser polishing and demonstrated its applicability even for 3D free-form surfaces. Similar to (large) area laser polishing, the smoothing of the surface can be carried out with both continuous and pulsed laser radiation. The circular laser beam is guided over the surface in a meandering pattern while using a laser beam diameter d_L and the scanning speed v_{scan} . In contrast to conventional laser polishing, however, the laser power/pulse energy used does not remain constant throughout the entire process. Laser power is switched on or off (or between various, different laser power levels) in a controlled manner depending on the location. Therefore, only selected areas on the surface are remelted and smoothed to pre-selected degrees. This results in a localized functionalization of the surface roughness. A reduction in micro-roughness significantly increases the ratio of directional to diffuse light reflection in particular [27]. After selective $L_{\mu}P$, the resulting surface thus exhibits a so-called dual- or multi-gloss effect (depending on the number of different process parameters), which is based on the contrast of matte, untreated areas to glossier, laser polished areas (see also Fig. 28).

2.2. Opto-mechanical set-up

An experimental set-up that enables the superposition of two laser beams is used as the opto-mechanical basis for this experimental investigation (Fig. 3). This opto-mechanical set-up was developed by Pütsch et al. [28] within the collaboration projects “FluidStruc” and “WaveShape” funded by the Volkswagen Stiftung. The laser beam source for pulsed laser radiation is an Nd:YAG fiber laser from SPI (model G3: SP-40P-HM-B-C-E-B). The wavelength of the emitted laser radiation is $\lambda_{puls} = 1064$ nm and therefore the infrared spectral range. The beam path of the fiber-coupled pulsed source ($\lambda_{puls} = 1064$ nm,

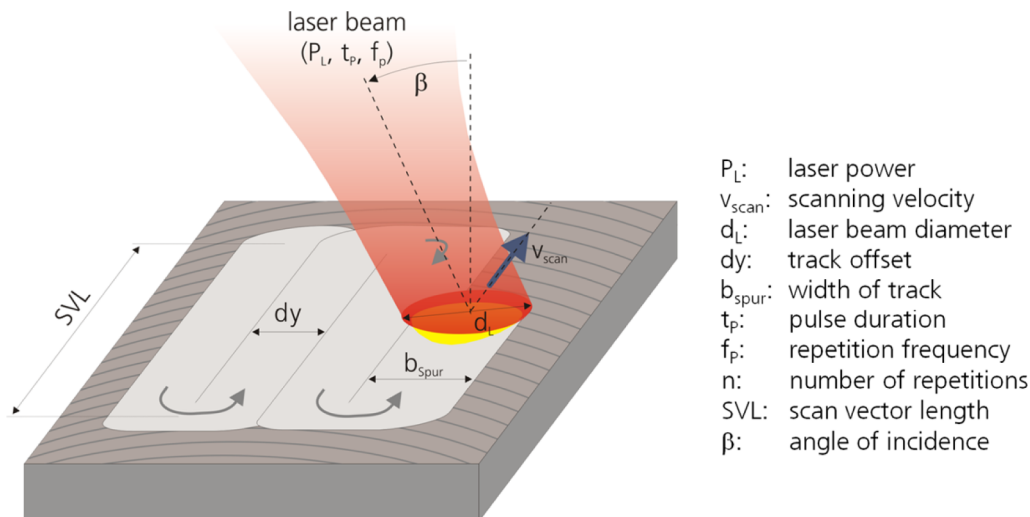


Fig. 2. Schematic of laser polishing by remelting a thin surface layer with pulsed laser radiation [35].

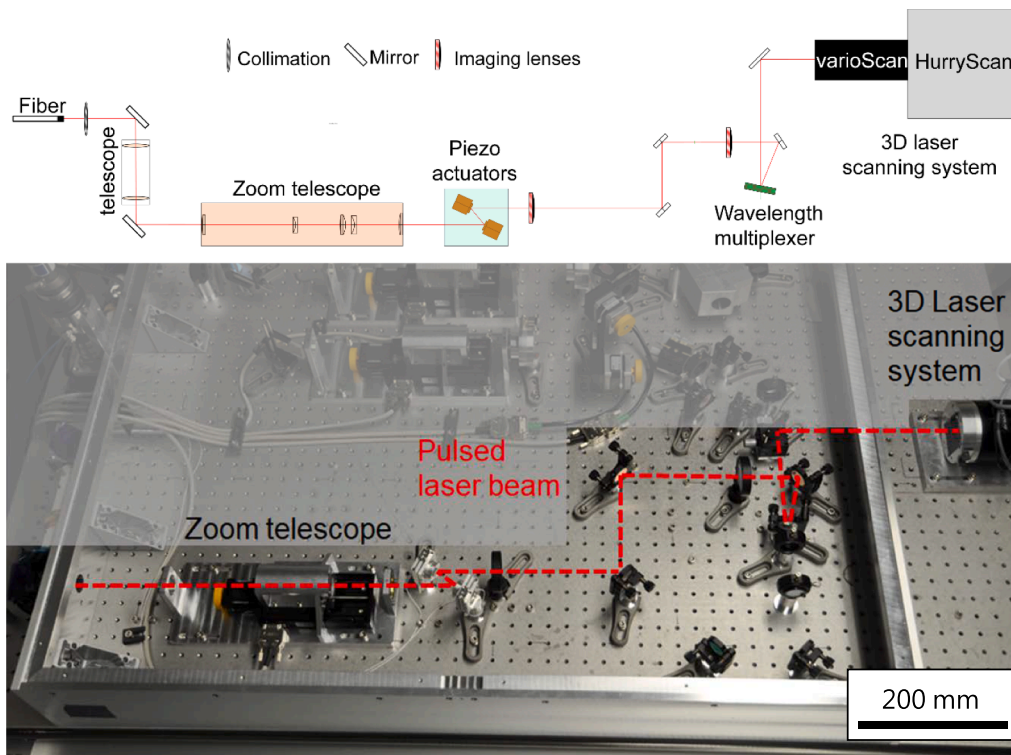


Fig. 3. Schematic (top) and photograph (bottom) of the experimental set-up.

$P_{\text{puls, max}} = 35 \text{ W}$, $t_p = 9\text{--}220 \text{ ns}$, $f_{p, \text{max}} = 400 \text{ kHz}$, $E_{\text{puls, max}} = 1.25 \text{ mJ}$, $P_{p, \text{max}} = 20 \text{ kW}$) is also comprised of a collimation and a fixed beam expander.

The laser beam is coupled into the optical set-up via an optical fiber and collimation, resulting in a collimated beam diameter of $d_L = 5.8 \text{ mm}$. The collimated laser beam is then guided through a telescope with a fixed magnification, which results in a collimated laser beam diameter of $d_L = 2.0 \text{ mm}$. By guiding the laser beam through a motorized zoom-telescope (developed by Fraunhofer ILT and TOS of RWTH Aachen University) the diameter of the collimated laser beam can be adapted in the range from $d_L = 0.36$ to 3.6 mm . This equates to an adaptable magnification from 0.18 to 1.8. For an additional two-dimensional transversal deflection of the pulsed laser beam, two one-dimensional piezo actuators are implemented, and placed orthogonally to each other. The piezo-driven mirrors enable a very accurate but small change (up to $\pm 2 \text{ mrad}$) in direction of the pulsed laser beam, with a frequency of up to two kilohertz. However, for this investigation, the movement of the laser beam is solely made by a ScanLab 3D laser scanning system. Additionally, two imaging lenses with a focal length of 250 mm are used in a 4f-arrangement to reduce residual beam divergence (relay telescope).

The 3D laser scanning system essentially consists of three components: a varioSCAN40 (type 63–magnification factor of the laser beam approx. 2.5), a HurryScan30 from Scanlab and an f-theta lens from Sill Optics GmbH & Co. KG (with a focal length of 163 mm). The varioSCAN40 enables dynamic and precise positioning of the laser focus along the optical axis. A hurrySCAN30 is used to enable fast and precise positioning of the laser beam focus on the workpiece. Those two components are controlled via an RTC4 interface card that is installed in a personal computer. In order to ensure a constant focus position of the laser beam in the processing field, an f-Theta lens (flat field objective) with a focal length of $f_{\text{theta}} = 163 \text{ mm}$ is used. The laser scanning system moves the laser beam over the workpiece surface at various scanning speeds v_{scan} , which are in the range of 500 mm/s and 2000 mm/s for this investigation.

In order to avoid oxidation of the remelted surface layer of the

workpiece, laser processing takes place in a process gas chamber filled with a mixture of inert gas and residual air. A manual x-z axis system enables positioning of the process gas chamber relative to a 3D laser scanning system. The positioning in y direction is done by manually moving the chamber on a sliding stage (Fig. 4). Argon is used as inert gas in all experimental investigations. The residual oxygen content of the process gas atmosphere is constantly monitored using an SGM5T oxygen measuring instrument from ZIROX and controlled to be equal or less than 100 ppm in all investigations.

2.3. Chemical composition of material and characteristics of initial surface

The material used for this investigation is the stainless, martensitic chromium steel AISI 410 (1.4006 or X12Cr13, Outokumpu brand name: Avesta 393 HCR), which is known for its good mechanical properties and very good weldability. A common application for this material are press plates for decorative laminates. Table 1 shows the chemical composition of this steel provided by Outokumpu.

The samples have a thickness of $5.0 (\pm 0.05) \text{ mm}$ (Fig. 7a). They were prepared by photochemical etching that created a distinguished, but not regular, surface structure, with heights in the range of $\pm 10 \mu\text{m}$ on the steel surface. After cleaning the surface of chemical residues from the structuring process, glass bead blasting was used to create a homogeneously matte surface. Fig. 5 and Fig. 6 show representative images of the initial surface topography measured by microscopy and WLI.

Glass bead blasting leads to a characteristic surface structure on meso-, micro- and nano-scales. Due to size and velocity distribution of the spherical glass beads used, “craters” of varying sizes/depths (between 20 and $40 \mu\text{m}$) are generated in a non-regular, statistical pattern on the surface. At the same time, non-spherical parts or glass splinters produce sharp-edged notches and scratches of varying sizes on the microscale. In particular, these micro-scratches and notches lead to a distinctly matte appearance of the surface.

Fig. 6 shows these characteristic surface features based on WLI measurements on meso- (left) and micro- (right) scale. These WLI

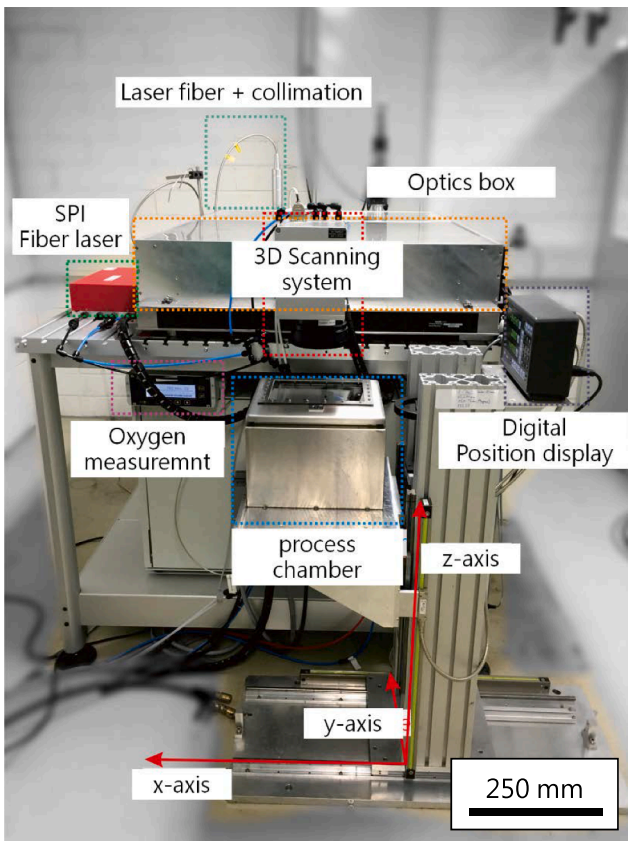


Fig. 4. Photograph of the experimental set-up for sample handling and laser processing.

Table 1

Tabular overview of chemical composition for Avesta 393 HCR (AISI 410) from data sheet of the supplier (in m.%).

Material\Element	C	Si	Mn	Cr	Fe
AISI 410	0.12	0.65	0.5	12.2	Bal.
Deviation	± 0.03	± 0.05	± 0.05	± 0.3	-

measurements were also used to calculate the surface roughness spectrum for the initial surface (straight black line in Fig. 11a).

Fig. 7 gives a visual impression of the initial surface and the resulting gloss for laser polished test fields. Each test field was laser polished with different process parameters and has a size of $10 \times 10 \text{ mm}^2$. The size of the samples was $250 \text{ mm} \times 165 \text{ mm} \times$

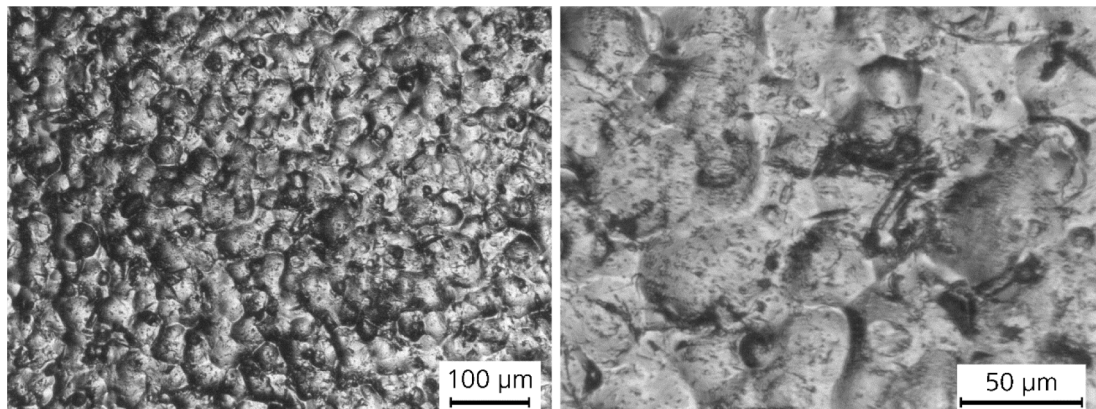


Fig. 5. Microscopic images in two different magnifications of initial surface topography.

5 mm.

2.4. Characteristics of the laser beam source

讨论高斯光束，平顶光束对抛光的影响

2.4.1. Intensity distribution

In most investigations for LµP a Gaussian intensity distribution (ID) is used. Otherwise, often a top-hat ID or an ID that lies geometrically “somewhere between” Gaussian or top-hat are used. Nüsser et al. [29] showed that by using a homogeneous (top-hat) ID a lower surface roughness is achieved than by using a near-Gaussian ID. Additionally, Nüsser et al. [29] report that using a circular, top-hat ID results in a lower surface roughness than using a square top-hat ID. Based on more detailed experimental investigations, Nüsser [2] comes to the overall conclusion that the influence of the ID (top-hat-shaped, Gaussian-like) on surface roughness is generally low. Using a top-hat-shaped ID often results in the same or a lower roughness than using a Gaussian-like ID. Concerning the geometry of the laser beam, Nüsser [2] finds that a lower meso-roughness was achieved using a quadratic laser beam cross-section in comparison to using a circular one, because the ID for the quadratic laser beam was more homogeneous than for the circular one. Therefore, due to the one-dimensional heat conduction for LµP, he hypothesizes that by using the same ID, the resulting surface roughness will presumably not depend on the focus geometry.

However, the ID still remains a key characteristic of the laser radiation used and should be characterized in order to achieve a high comparability between experiments. Therefore, prior to laser processing, the pulsed laser beam was characterized by a MicroSpotMonitor (MSM) of the company Primes, especially in and close to its focal plane. Using the MSM, beam parameters of focused laser beams can be analyzed by a CCD sensor after imaging the laser beams, which are attenuated via various beam splitters and neutral density glass filters. Additionally, an integrated z-axis enables the laser beam to be imaged in different planes, so that characteristics of the laser beam such as ID and laser beam diameter can be determined.

Fig. 8 shows a representative geometry and ID of the laser beams used within this investigation. The diameter of the pulsed laser beam is approx. $d_L = 120 \mu\text{m}$ (Fig. 8a) at $\lambda_{em} = 1064 \text{ nm}$, $P_L = 15 \text{ W}$, Waveform 0 and $f = 30 \text{ kHz}$ with a M^2 of approx. 3.2. The corresponding ID is depicted in Fig. 8b and c. The resulting Rayleigh length was measured to be $z_R = 3.2 \text{ mm}$, while beam divergence was approx. $\theta_f = 37 \text{ mrad}$. Therefore, this ID is neither a pure Gaussian nor a pure top-hat ID. Furthermore, it has no distinctive peaks, so a good overall laser polishing performance can be expected.

2.4.2. Pulse-to-pulse stability

The Pulse-to-pulse stability (PPS) is a characteristic of the laser beam source and may vary depending on the actual operating point. PPS is a measure for the similarity of laser pulses generated by a laser

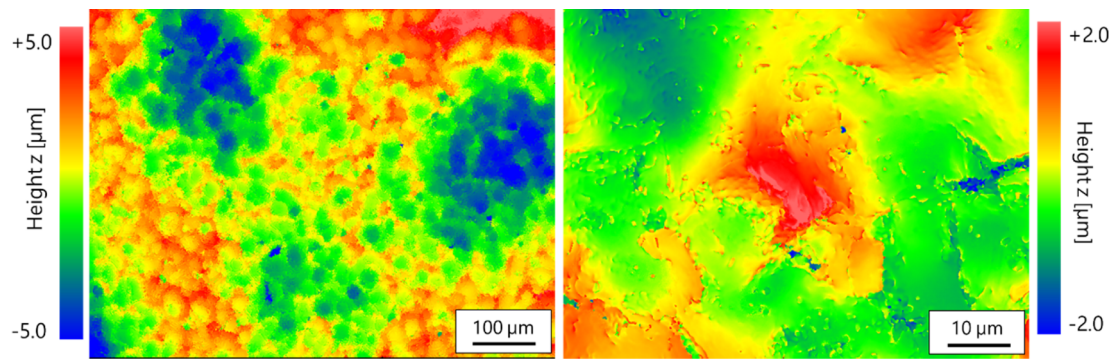


Fig. 6. Representative WLI images of initial surface topography in two different magnifications.

beam source. Therefore, it can be seen as an intrinsic error of operation for all laser experiments with pulsed laser radiation and should be as small as possible. Consequently, Temmler [4] hypothesizes that an inferior PPS might be responsible for polishing results that are of overall lower quality. Nüsser [2] finds that the PPS of the laser beam source must be “sufficiently high” in order to achieve a homogeneously remelted surface. He achieves such surfaces with a maximum deviation of the pulse energy of $\pm 25\%$. This means that no single pulse deviates more than 25% from the average pulse energy. Nüsser [2] achieved a comparatively high reproducibility of the laser polishing process with an overall standard deviation of 3–6%.

To measure the pulse-to-pulse stability (PPS), an oscilloscope RTE1024 (Rohde & Schwarz) in combination with a photodiode DET10A/M (Thorlabs) are used. In order to determine the PPS 100.000 pulses are measured by the photodiode. For that, the laser beam was directed into a laser power measurement device (PowerMax30 - PM30 by coherent). The photodiode was positioned at an angle of approx. 45° and at a distance of approx. 50 mm relative to the incident laser beam on the absorbing surface of the PM30. Therefore, a small fraction of the reflected laser beam was measured by the photodiode and then analyzed by an oscilloscope. At the same time, the average laser power was measured in order to correlate the average laser power with pulse energy at a given pulse frequency (which was also measured by the oscilloscope). Pulse energy for each pulse was then calculated by integrating pulse intensity over pulse duration for each pulse (internal measurement program of RTE1024). Subsequently, pulse count and pulse energy were normalized with a resolution of 1/1250 (norm. count) and 0.025% (norm. pulse energy) respectively. The histogram plot in Fig. 9a shows normalized pulse count as a function of

normalized pulse energy. The standard deviation σ of this Gaussian like pulse energy distribution is approx. $\sigma = \pm 0.6\%$, while 100% of all pulses are in a range of ΔE_p of $\pm 2.57\%$ of the average pulse energy.

A high PPS enables the laser polishing process to be carried out close to the ablation threshold. Compared to a significantly smaller PPS, this increases the effective melting time on the one hand and reduces the probability of material removal on the other (e.g. by individual laser pulses with significantly higher average pulse energy). Therefore, it is expected that highly reproducible and homogenous results are achieved, if material and material quality are sufficiently suited. This should effectively reduce the formation of undesired structures like craters and holes due to material ablation and lead to higher degree of statistical certainty for this investigation.

2.4.3. Waveform and PRF₀ frequency

For the laser beam source, pulse duration or emission length is changed by selecting a specific, preset waveform. A cut-off frequency (PRF₀) is assigned for each preset waveform. The maximum pulse energy is available up to this PRF₀-frequency (Fig. 10a). Basically, the shorter the pulse duration, the smaller the maximum pulse energy and the higher the corresponding PRF₀-frequency. At pulse frequencies higher than the respective PRF₀-frequency, the maximum pulse energy is reduced, since the maximum laser power is limited. Thus, only at the PRF₀-frequency are both maximum pulse energy and maximum average laser power available at the same time.

Pulse frequency will be one of the main process parameters investigated. Therefore, the shape of laser pulses is measured as function of pulse frequency. The same devices used for the determination of PPS are also used to measure the time-dependent shape of laser pulses.

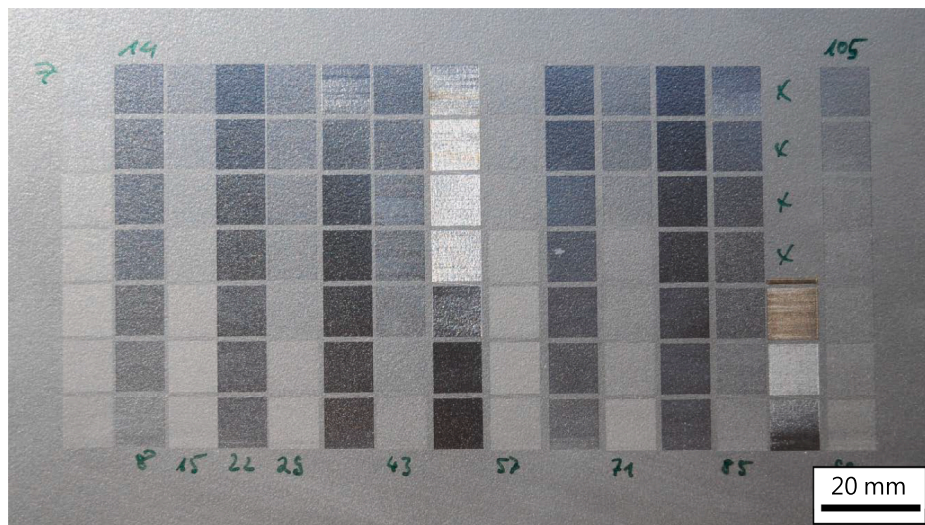


Fig. 7. Photograph of a prepared specimen with 105 test fields for L μ P in a regular pattern. The field size is 10x10 mm².

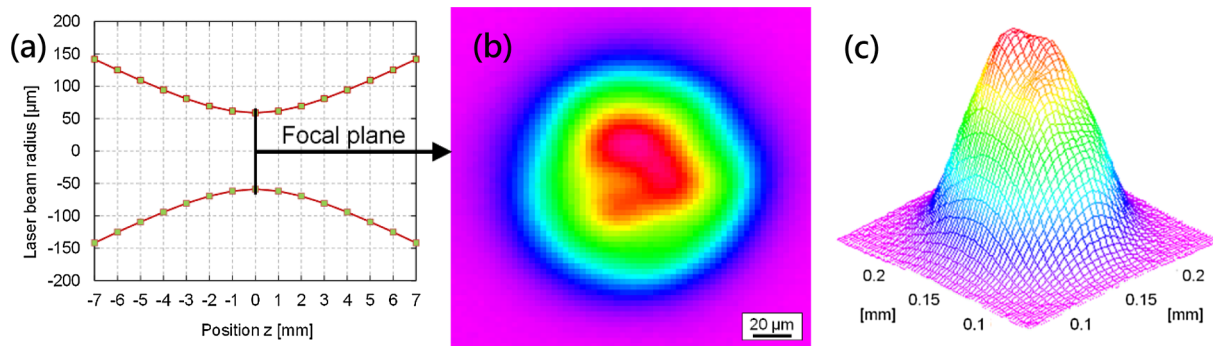


Fig. 8. (a) Caustic of laser beam, (b) 2D-Intensity distributions (ID) of pulsed laser beam in plane of processing, (c) 3D intensity distribution of pulsed laser beam with $d_{L,puls} = 120 \mu\text{m}$.

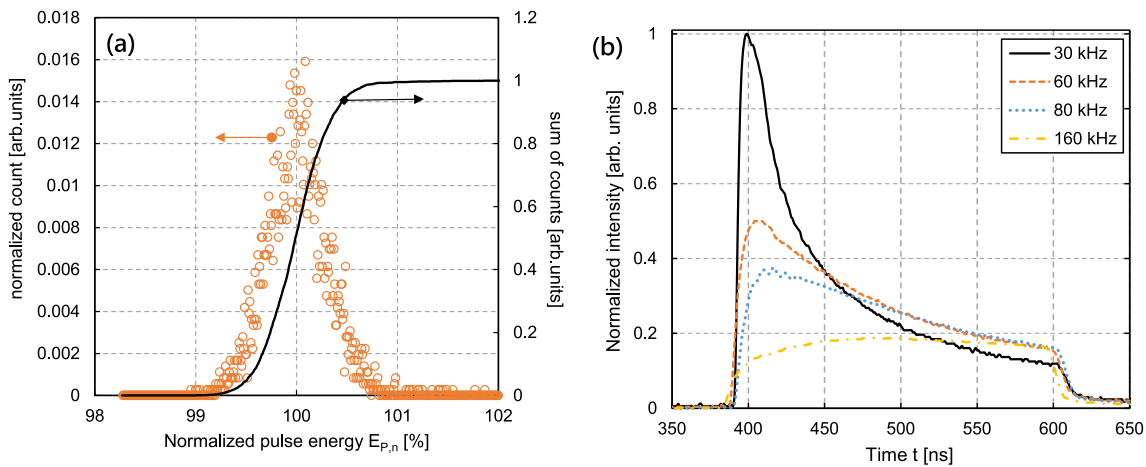


Fig. 9. (a) PPS for SPI G3 at 100% laser power and pulse frequency of 30 kHz at WV0; (b) shape of laser pulses for Waveform 0 at different pulse frequencies for $t_p = 220 \pm 10 \text{ ns}$.

Fig. 9b shows that the pulse shape depends significantly on the pulse frequency. With increasing pulse energy, the intensity peak at the beginning of a laser pulse (within in the first approx. 50 ns) decreases with increasing pulse frequency. The higher the pulse frequency, the more the pulse shape resembles a rectangular shape, which is particularly pronounced at a pulse frequency of 160 kHz. This means that the intensity of the laser radiation is almost constant over the entire pulse duration. Therefore, the pulse duration used in this case is not the full width at half maximum, but the duration of laser emission. This duration of laser emission is $t_p = 220 \text{ ns}$ and almost the same for all pulse frequencies.

In addition, a change in the waveform not only changes the pulse

duration but also the pulse shape as shown in Fig. 10b. The specified pulse duration refers essentially to the duration of laser emission, i.e. how long the laser resonator is pumped by the laser diodes. Further details and special features of the laser system used can be found in the corresponding manuals for the laser systems SPI G3 and SPI G4.

Table 2 gives an overview of the specifics for each waveform regarding its PRF₀-frequency, pulse duration and maximum pulse energy. The maximum peak power can be calculated by dividing maximum pulse energy by pulse duration. Therefore, this laser beam source enables an investigation of pulse durations from 10 ns to 220 ns and pulse frequencies up to 250 kHz. Both pulse duration and pulse frequency have yet to be investigated in this range.

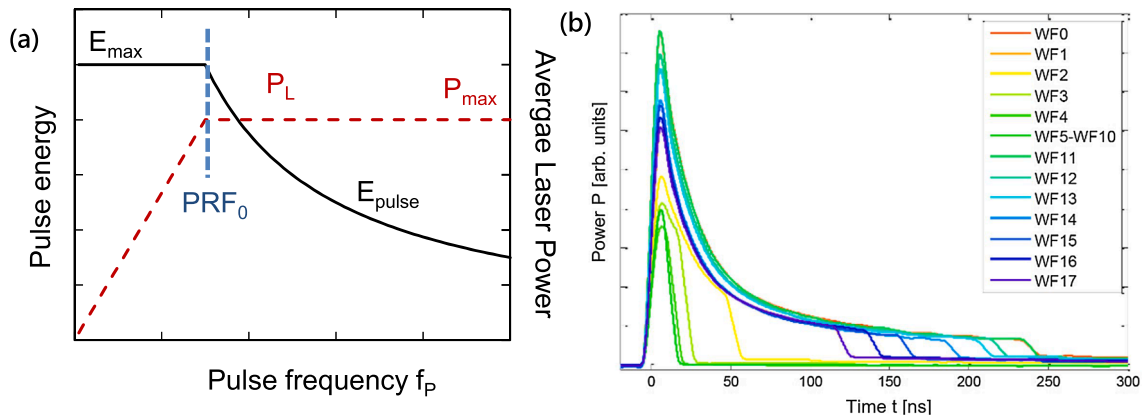


Fig. 10. (a) Schematic of relationship between pulse energy, laser power and pulse frequency; (b) shape of laser pulses for different preset waveforms.

Table 2
Overview of waveforms, pulse frequencies, pulse duration and available maximal pulse energy.

Waveform No.	PRF ₀ f _p [kHz]	Pulse duration t _p [ns]	Max. Pulse energy E _{p,max} [mJ]
0	30	220	1.20
1	47	130	0.75
2	76	60	0.46
3	145	30	0.24
4	230	20	0.15
5	250	10	0.14

2.5. Surface analysis

For evaluation of a surface, often surface topography is measured by means of stylus methods or white light interferometry. Based on the measurement results, the average surface roughness Ra (for lines) or Sa (for areas) is determined. For a more detailed analysis of surface roughness, the spectral composition of the roughness in the form of a roughness spectrum (Sa-spectrum) is analyzed, presented and discussed. Willenborg [3] describes for the first time how WLI measurements are used to calculate a Sa-spectrum. The roughness is analyzed as a function of the spatial wavelength using a phase-correct profile filter. Temmler [4] distinguishes three different characteristic intervals in a Sa-spectrum: micro-roughness in the range of $\lambda = 0.625\text{--}10\ \mu\text{m}$, meso-

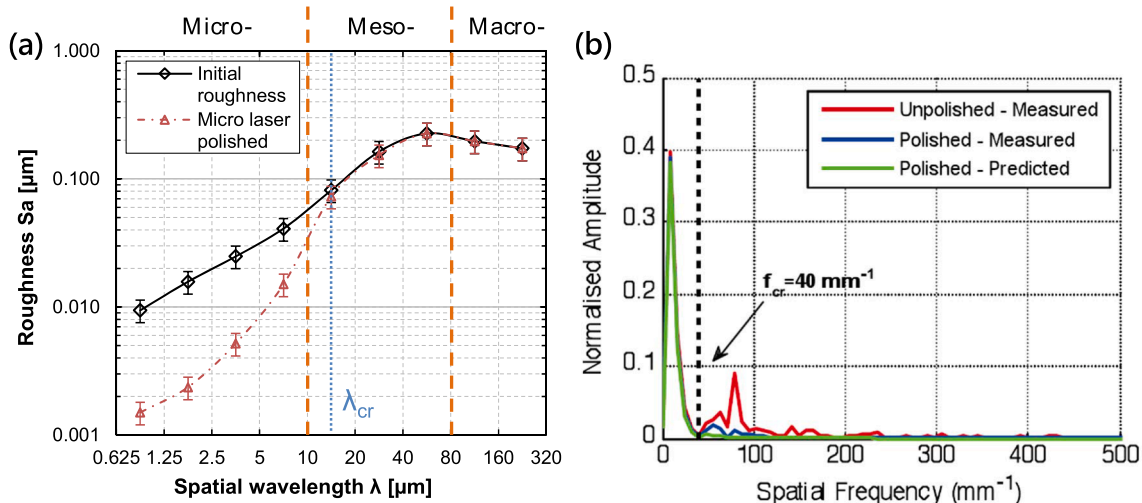


Fig. 11. (a) Sa-roughness spectrum [4], (b) Spatial frequency spectrum [11]

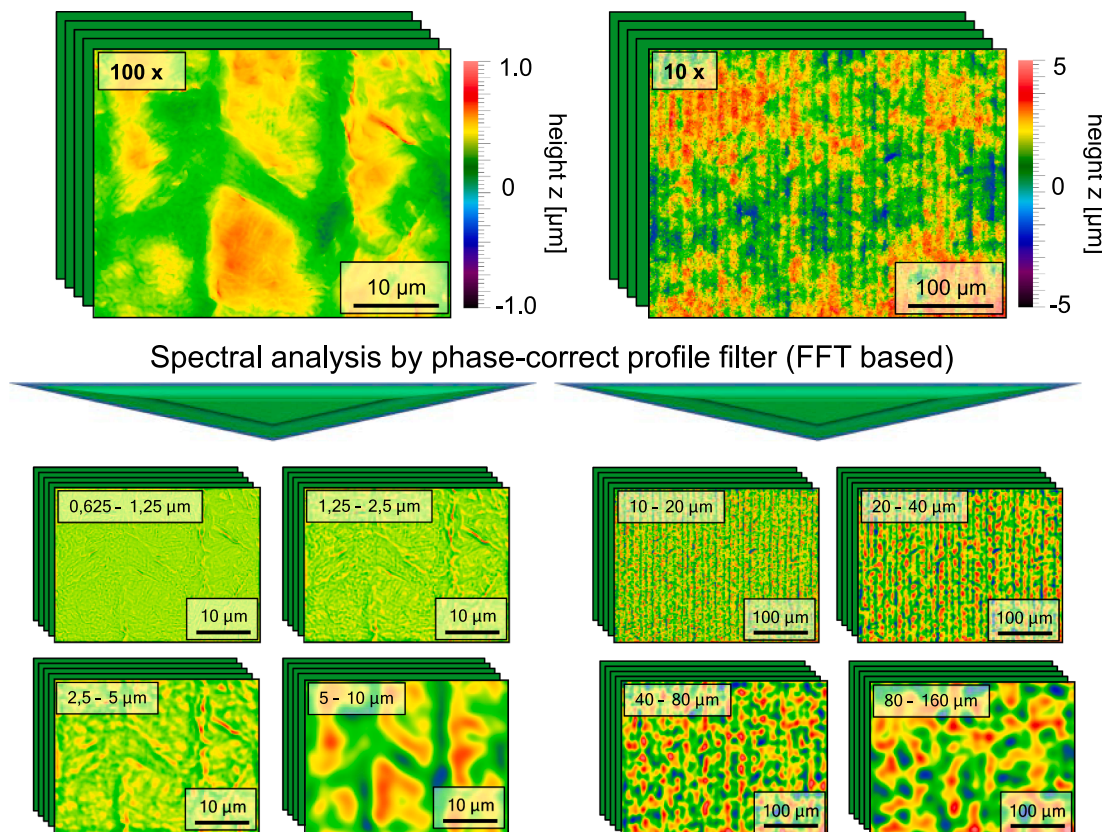


Fig. 12. Schematic for spectral analysis of surfaces based on different WLI measurements at two different magnifications.

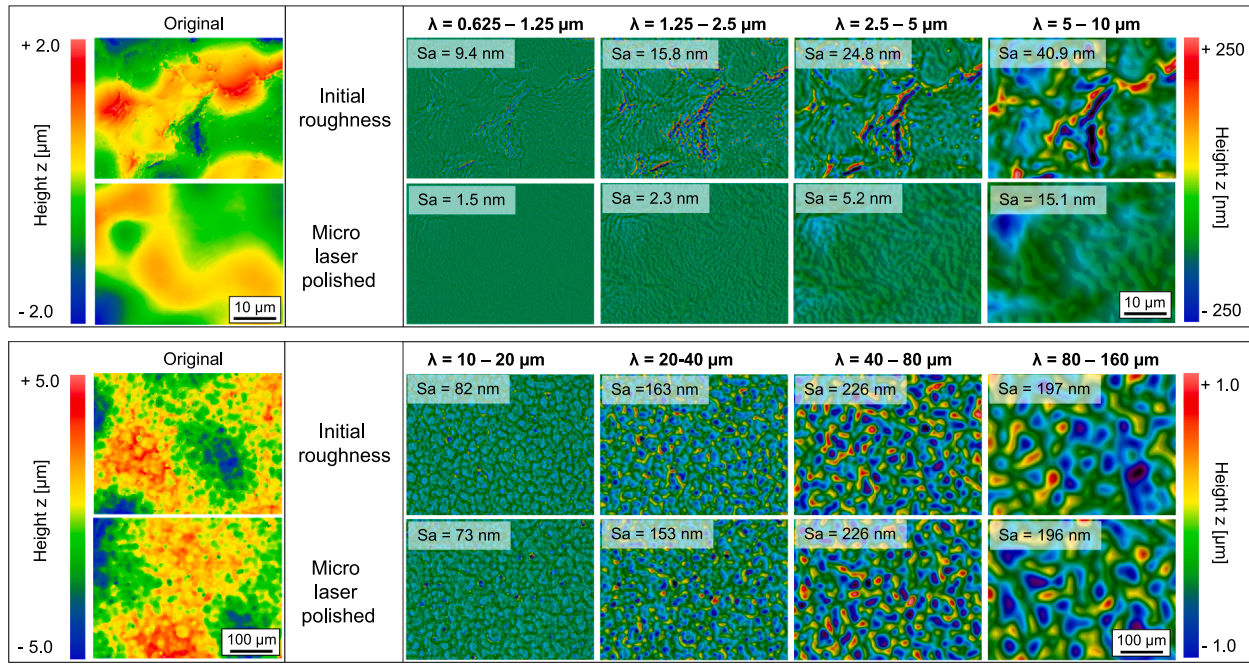


Fig. 13. Comparison of initial and laser polished surface for different wavelength intervals before and after bandpass filtering.

roughness in the range of $\lambda = 10\text{--}80 \mu\text{m}$ and macro-roughness in the range of $\lambda = 80\text{--}320 \mu\text{m}$ (Fig. 11a).

Frequently, the roughness is also displayed as a function of spatial frequency (spatial frequency spectrum, Fig. 11b). Perry [11], for example, measures surfaces using a stylus method (2D) or white light interferometry (WLI-2D or 3D). Subsequently, the amplitude for each spatial frequency f is determined using a Fast Fourier Transform (FFT). Using a frequency spectrum for roughness analysis, Chow et al. [12] point out that mainly high spatial frequencies are smoothed by $\text{L}\mu\text{P}$. Based on their analysis of roughness wavelength spectra, Temmler et al. [26] point out analogously that $\text{L}\mu\text{P}$ predominantly smooths short spatial wavelengths. In this context, Perry [11] introduces the often and widely used critical spatial frequency f_{cr} . This describes the lowest spatial frequency whose amplitude is effectively smoothed compared to the initial state. Similarly, the longest spatial wavelength is referred to as the critical spatial wavelength λ_{cr} [30].

For this investigation, a white light interferometer (WLI, NewView 7300 from Zygo, is used to measure laser polished surfaces without any mechanical contact. The spatial resolution is up to $dx = dy = 0.1125 \mu\text{m}$. The optical resolution of the height or z -direction is in the order of $dz = 0.1 \text{ nm}$. Fig. 12 shows a schematic representation of a spectral analysis based on WLI measurements from two different magnifications. The surface of each laser polished area is measured at a minimum of five different locations using two different spatial resolutions of $dx_{100x} = 0.1125 \mu\text{m}$ and $dx_{10x} = 1.125 \mu\text{m}$. The size of each measurement is $480 \times 640 \text{ pixels}$ (Fig. 12 top). This results in five measurements for each field of view of $\text{FoV}_{100x} = 54 \mu\text{m} \times 72 \mu\text{m}$ (100x) and $\text{FoV}_{10x} = 540 \mu\text{m} \times 720 \mu\text{m}$ (10x) respectively. Discrete spatial wavelength intervals are defined for each spatial resolution. For each spatial resolution, the lowest wavelength limit results from the fact that the wavelength must be at least four to five times as large as the spatial resolution of the measurement. Therefore, at least four or five discrete sampling points would describe a sine wave with the length of the smallest wavelength limit ($\lambda_{\text{min,mag}} \approx 5 dx_{\text{mag}}$). The upper wavelength limit for each spatial resolution is about a quarter of the measuring field size, so that at least four wavelengths can be evaluated within this measuring field ($\lambda_{\text{max,mag}} \approx 0.25 \text{ FoV}_{\text{mag}}$). For the magnifications used, this results in four wavelength limits ($\lambda_{\text{min,100x}} \approx 0.5625 \mu\text{m}$; $\lambda_{\text{max,100x}} \approx 13.5 \mu\text{m}$; $\lambda_{\text{min,10x}} \approx 5.625 \mu\text{m}$; $\lambda_{\text{max,10x}} \approx 135 \mu\text{m}$).

Between these upper and lower wavelength limits, the wavelength limits are doubled or halved, respectively. For historic reasons, the doubling and halving of the wavelength interval limits starts at $10 \mu\text{m}$ and thus defines the rest of the wavelength intervals. This leads to four discrete spatial wavelength intervals for each magnification (Fig. 12 bottom).

For $\text{FoV}_{100x} = 54 \mu\text{m} \times 72 \mu\text{m}$ and a spatial resolution of $dx_{100x} = 0.1125 \mu\text{m}$, these are $0.625\text{--}1.25 \mu\text{m}$; $1.25\text{--}2.5 \mu\text{m}$; $2.5\text{--}5 \mu\text{m}$ and $5\text{--}10 \mu\text{m}$.

For $\text{FoV}_{10x} = 540 \mu\text{m} \times 720 \mu\text{m}$ and a spatial resolution of $dx_{10x} = 1.125 \mu\text{m}$, these are $10\text{--}20 \mu\text{m}$; $20\text{--}40 \mu\text{m}$, $40\text{--}80 \mu\text{m}$ and $80\text{--}160 \mu\text{m}$ (although $160 \mu\text{m}$ is slightly longer than $\lambda_{\text{max,10x}} \lambda_{135 \mu\text{m}}$). Therefore, the maximal spatial wavelength for roughness analysis is limited to $\lambda_{\text{max}} = 160 \mu\text{m}$, while the minimum spatial wavelength is $\lambda_{\text{min}} = 0.625 \mu\text{m}$. Overall, these wavelength limits result essentially from the lateral resolution of the magnifying objectives used in the white light interferometer.

A Gauss weighted function similar to ISO 11,562 is used for a discrete convolution with the surface profile in order to achieve a spectral analysis of the measured surface⁵. In comparison to the original surface, the filtered surface shows no phase-shift and therefore no dislocation [26]. In principal, the limits for each spatial wavelength interval act as cut-off frequencies for a Gauss weighted bandpass filter. After these specific bandpass filters were applied to each measurement, the average surface roughness was calculated using the standard definition of surface roughness Sa (Fig. 13)⁶. Fig. 13 shows an exemplary comparison of an initial, unpolished surface and a laser polished surface for different wavelength intervals before and after bandpass filtering. Fig. 13 is subdivided into two parts for micro-roughness (Fig. 13 top- $\lambda = 0.625 \mu\text{m}\text{--}10 \mu\text{m}$) and meso-roughness (Fig. 13 bottom- $\lambda = 10 \mu\text{m}\text{--}160 \mu\text{m}$). Surface roughness was calculated for each wavelength interval. For each individual wavelength interval, a comparison of the

⁵ Gaussian weighted function of the form: $Ae^{\left(\frac{\sqrt{x^2+y^2}}{\lambda}\right)^2}$, where A is Amplitude, and λ is cut-off frequency.

⁶ Standard Definition of arithmetical mean of surface roughness $Sa = \frac{1}{A} \iint_A |z(x, y)| dx dy$

initial surface and the laser polished surface is shown. The calculated surface roughness values are the basis for a roughness spectrum (Sa-spectrum). Each point within a Sa-spectrum is based on the mean average and the standard deviation for at least three independent surface roughness measurements and analyses (Fig. 11a).

Because of the duplication of spatial wavelength limits and due to a wide range of surface roughness amplitudes, the spatial roughness is illustrated logarithmically. Each roughness value on the y-axis represents therefore the roughness for the specific wavelength interval. Lower and upper limits for this specific wavelength interval are given on the x-axis. Fig. 13 can be seen as graphical illustration of a Sa-spectrum (Fig. 11a) without statistical error analysis.

2.6. Process parameters and scope of this investigation

2.6.1. Fluence

Poprawe [31] points out that pulse duration and intensity are the process parameters with the greatest influence on the resulting surface roughness. The fluence F is defined as the quotient of the pulse energy E_p and the interaction zone between laser radiation and material surface. The pulse energy is usually given by the quotient of average laser power P_L and pulse repetition frequency f_p . The interaction zone is calculated to be the area A_{int} covered by a laser beam with a diameter d_L . $F = E_p \cdot A_{int}^{-1}$ with $E_p = P_M \cdot f_p^{-1}$ and $A_{int} = 0.25 \cdot (\pi \cdot d_L^2)$ (or an equivalent area for non-circular laser beams).

$$F = \frac{4 \cdot P_L}{f_p \cdot \pi \cdot d_L^2} \quad (4.1)$$

The fluence significantly influences the temperature-time history during L μ P⁷. Therefore, a fluence and a set of process parameters for each material that leads to a minimal roughness is usually determined

⁷ Chang et al. [32] seems to quantifiably confirm the significant qualitative influence of fluence on the resulting surface roughness. However, the publication by Chang et al. [32] is from our point of view only of very limited, practical and scientific relevance. This is due to the fact that the calculation of the Rayleigh length, which is used for all of the subsequent calculations, is incorrect. The correct calculation of the Rayleigh length would be: $z_R = \omega_0 \theta_0^{-1} = \pi \omega_0^2 (M^2 \lambda)^{-1} = 709.17 \mu\text{m}$ ($\omega_0 = 16.3 \mu\text{m}$, $M^2 = 1.1$ and $\lambda = 1.070 \mu\text{m}$). In contrast to $z_R = 0.78 \mu\text{m}$ calculated by the authors, this is a difference of approximately three orders of magnitude. Therefore, the values given for focus offset and the resulting laser beam diameter are also incomprehensible and highly likely to be incorrect. This also applies to the calculations and graphs, which were created on the basis of the derived fluences. In addition to this publication, the publications partially based on the same or similar calculations should be checked and verified very carefully. Even moderate process parameters specified in this publication (e.g. $P_L = 100 \text{ W}$, $v = 400 \text{ mm/s}$, $t_p(D) = 14 \mu\text{s}$, $f_p(FQ) = 25 \text{ kHz}$; $d_L(SS) = 38 \mu\text{m}$, $F = 352.7 \text{ J/cm}^2$, $EP = 4 \text{ mJ}$) appear unsuitable for laser polishing. For example, Vadali (2013) uses these process parameters ($P_L = 3.38 \text{ W}$, $v = 224 \text{ mm/s}$, $t_p(D) = 1.6 \mu\text{s}$, $f_p(FQ) = 40 \text{ kHz}$; $d_L(SS) = 37.5 \mu\text{m}$, $F = 7.43 \text{ J/cm}^2$, $E_p = 0.0845 \text{ mJ}$) and achieves a significant smoothing of a metal surface. On the one hand, based on the authors' experience regarding macro-polishing with cw radiation, we can state that massive material ablation already occurs using this set of process parameters (which the authors do not mention). On the other hand, the same material has already been examined in detail by (Liebing, 2010). An effective smoothing of the roughness is already achieved at fluences of approx. $F = 4 \text{ J/cm}^2$ (at $t_p = 350 \text{ ns}$, $d_L = 250 \mu\text{m}$, $E_p = 7.85 \text{ mJ}$). Likewise, Chang et al. [32] contradicts numerous publications in the field of laser micro-polishing of steel materials. A set of process parameters like $d_L = 30 \mu\text{m}$, $P_L = 100 \text{ W}$, $v = 50 \text{ mm/s}$, $dy = 0.05 \text{ mm}$ (also mentioned in a publication of Chang et al.) will lead surely to massive evaporation of material. Usually these process parameters are used for a laser beam diameter of approx. $d_L = 250 \mu\text{m}$ instead of $d_L = 30 \mu\text{m}$. Therefore, doubts and caution are also justified concerning the results of the publications of Chang et al. [33] and Chang et al. [34] on surface quality, microstructure, and mechanical properties of SKD 61 tool steel after laser polishing. Both of the later publications are based on similar or slightly adapted calculations from Chang et al. [32].

experimentally. For this purpose the fluence is adapted to the other process parameters and typically the pulse energy (i.e. average laser power) is varied systematically based on test fields for L μ P. The smallest roughness and therefore the laser polishing fluence F_{pol} is determined by roughness measurements, e.g. by WLI. A characteristic trend of surface roughness as function of fluence is that the decrease of initial roughness correlates with increasing fluence. After reaching a local roughness minimum, however, the roughness increases again with a further increase of fluence due to localized material evaporation [35]. If fluences are used that lead to material evaporation, the resulting surface roughness is often greater than the initial surface roughness [36].

Due to the characteristics of the laser beam source, as discussed in paragraph 4.4.3, the pulse energy can be increased up to $E_{p,max} = 1.2 \text{ mJ}$ for a laser beam diameter as small as $d_L = 100 \mu\text{m}$. Therefore, the maximum Fluence is 10.6 J/cm^2 . This fluence is well above the fluence usually needed for laser polishing of steels [35].

2.6.2. Pulse duration

The general assumption is that an increasing pulse duration leads to an increasing melt duration. A longer period of time is therefore available during which the roughness can "flow out" under the influence of the surface tension of the melt pool, resulting in a smoother surface. Willenborg [3] finds that different kinds of roughness (micro- or macro-roughness) are smoothed more or less effectively based on the pulse duration (using hot work steel AISI H11). When using longer pulse durations (comparison $t_p = 16 \text{ ns}$ and $t_p = 480 \text{ ns}$), longer spatial wavelengths are smoothed. However, in a singular experiment, it was also shown that with a short pulse duration ($t_p = 16 \text{ ns}$), a smaller micro-roughness could be achieved than with a longer pulse duration ($t_p = 480 \text{ ns}$). Perry et al. [37] find that with a pulse duration of $t_p = 650 \text{ ns}$ the roughness of nickel samples is smoothed more effectively than with a pulse duration of $t_p = 300 \text{ ns}$. Vadali et al. [15] achieve a significantly greater roughness reduction using a pulse duration of $t_p = 3.60 \mu\text{s}$ (72%) in comparison to a pulse duration of $t_p = 0.65 \mu\text{s}$ (21%). In accordance with these results, Nüsser [2] reports on similar findings and states that pulse durations should be as long as possible in order to smooth the longest possible critical spatial wavelength and create the lowest possible number of surface defects. Nevertheless, for materials where microstructures are to be expected after L μ P (e.g. martensite needles etc.), a short pulse duration must be chosen for the lowest possible micro-roughness, since the micro-roughness increases with the pulse duration.

However, the works of Temmler [4], Hafiz et al. [22], and Chen et al. [23] seem to contradict these results. Temmler [4] conducted studies on the influence of pulse duration on surface roughness for the hot work steel AISI H11. A result of this investigation was that with a shorter pulse duration, a lower micro roughness was achieved and a longer critical spatial frequency was smoothed than with a longer pulse duration. This contradiction was resolved to some extent since Temmler [4] referred to two potential causes. Both intensity distribution (ID) and pulse-to-pulse stability (PPS) of the laser beam sources used were significantly different. Therefore, PPS and ID probably had the larger influence compared to the difference in pulse duration. Hafiz et al. [22] use a pulse duration in the picosecond regime, a pulse frequency in the megahertz range, and a laser beam diameter of approx. $d_L = 35 \mu\text{m}$. They achieved a reduction of surface roughness from $Sa = 0.435 \mu\text{m}$ to $Sa = 0.127 \mu\text{m}$ for IN 718. This is remarkable since very short pulse durations ($t_p = 10.5 \text{ ps}$) and small fluences were used ($F = 0.19 \text{ J/cm}^2$) which nonetheless led to an effective smoothing of spatial frequencies lower than 10 mm^{-1} .⁸ Therefore, Hafiz et al. [22] demonstrated a

⁸ For this case, in the model of Perry [11], the pulse duration can no longer be equated with the melt duration for calculating the critical spatial frequency. Rather, it must be noted that with the combination of pulse frequency, scanning speed and laser beam diameter used, an area with the size of the laser beam

feasible way to achieve an effective smoothing of surfaces almost independent on the pulse duration used. Chen et al. [23] use similar process parameters ($t_p = 10$ ps) and a multi-step process to reduce surface roughness for ASP 23 mold steel from $Sa = 0.22 \mu\text{m}$ to $Sa = 0.158 \mu\text{m}^9$.

This work investigates pulse durations from $t_p = 9$ ns to $t_p = 220$ ns in combination with pulse frequencies between 20 kHz and 240 kHz. Both pulse duration and pulse frequency have yet to be investigated in this range.

2.6.3. Pulse overlap, track offset, laser beam diameter, number of remeltings

The spatial distance between successive laser polishing tracks perpendicular to the scanning direction is defined as track offset dy . The absolute pulse overlap is defined as the overlapping area of successive laser pulses, while the relative pulse overlap is the absolute pulse overlap in relation to the interaction area covered by a laser beam with a diameter d_L . Furthermore, the number of passes n are a measure for how often a surface was remelted. Altogether, these process parameters determine how often each point of a laser polished surface was remelted on average.

Overlap of subsequent laser pulses with a circular geometry and a diameter d_L in scanning direction dx is given in Eq. (4.2). The offset dx is calculated as the quotient of scanning velocity and pulse frequency ($dx = v_{\text{scan}} \cdot f_p^{-1}$). Therefore, the pulse-to-pulse distance (PPD) is $dx = 20 \mu\text{m}$ for e.g. a pulse frequency of $f_p = 50$ kHz and a scan speed of $v_{\text{scan}} = 1000$ mm/s. For y-direction or secondary scan direction the overlap is calculated analogously by substituting dx for dy .

$$O(dx, dL) = 2 \frac{d_L^2 \cdot \cos^{-1}\left(\frac{dx}{d_L}\right) - dx \cdot \sqrt{d_L^2 - dx^2}}{d_L^2 \pi} \quad (4.2)$$

$$n_x = \frac{1}{1 - O(dx, dL)}; n_y = \frac{1}{1 - O(dy, dL)} \quad (4.3)$$

Based on the respective overlap in x-direction and y-direction, the average number of remelting cycles can be calculated using Eq. (4.3). By multiplication of $n_x \cdot n_y$ it is possible to estimate how often a point on the laser-polished surface was remelted on average. In this context, Perry [11] came to the conclusion that a pulse overlap in scanning direction of up to 87.5% had a positive effect on the reduction of roughness¹⁰. Therefore, he used a pulse overlap of more than 80% as standard. Furthermore, he also concluded that roughness is not significantly reduced by an increasing number of passes, i.e. repeating the

(footnote continued)

diameter is exposed more than 13,000 times to laser pulses. Even when using picosecond pulses, this leads to a significant, local heat accumulation, which on the one hand leads to an extension of the effective melt duration and on the other hand significantly reduces the fluence required for remelting. Furthermore, the temporal pulse-to-pulse distance is approx. 135 ns. Similarly, no significant smoothing of spatial frequencies smaller than 10 mm^{-1} could be achieved in investigations with a pulse duration in the range of $t_p = 135$ ns. Therefore, it can be assumed that the melt duration of the melt pool is significantly longer than 135 ns. This leads to the conclusion that the laser polishing process with picoseconds of Hafiz et al. [22] is no longer a discrete micro-polishing process, but a (quasi-) continuous macro-polishing process. The difference to the macro-polishing process is that a melt pool continues to exist for all times during the macro laser polishing process. In this case, an interaction time t_{int} of laser radiation and material that can be calculated as laser beam diameter d_L divided by scanning velocity v_{scan} , is a better approximation for the order of magnitude of the melt duration ($t_{\text{int}} = 1.75$ ms).

⁹In principle, this process can also be assumed to be a macro polishing process with a continuously existing melt pool. A further indication is also that a pronounced strip structure is visible at the distance of the track offset, which is in particular characteristic for a continuous polishing processes.

¹⁰For the chosen process parameters: ($d_L = 75 \mu\text{m}$, $v_{\text{scan}} = 40$ 340 mm/s, $f_p = 4$ kHz, $t_p = 650$ ns, $F = 5.47 \pm 0.2 \text{ J/cm}^2$).

laser polishing with the same process parameters. In addition, Perry [11] found that multiple passes with a fluence smaller than the laser polishing fluence does not result in the same roughness reduction as the laser polishing fluence. Nüsser [2] found that pulse overlap in the scanning direction had almost no influence on the minimum achievable roughness, but the required laser polishing fluence decreases with increasing pulse overlap¹¹. In addition, Nüsser [2] found that the influence of the pulse overlap on the required laser polishing fluence was larger than that of the track offset and hypothesized that this was due to locally different preheating conditions. Furthermore, he found that a decrease of track offset led to a smoother micro-roughness. Due to the more frequent remelting of the surface, surface defects caused by previous remelting cycles were significantly smoothed. With regard to the number of passes, Nüsser [2] found that the influence of the number of passes on surface roughness depended significantly on the process gas atmosphere and the proportion of residual oxygen contained therein. Nevertheless, the tendency was noted that the roughness increases with the number of passes ($n > 1$).

The pulse frequency of the laser beam sources determines the temporal distance of two subsequent laser pulses and the number of laser pulses to hit the surface per unit of time. In combination with scanning velocity v_{scan} , the pulse frequency not only determines the temporal pulse-to-pulse distance (PPD) dt of successive laser pulses but also the spatial PPD dx in scanning direction. Besides fluence F , the combination of the process parameters pulse frequency f_p , scanning velocity v_{scan} , and laser beam diameter d_L significantly influence the temporal and spatial temperature curve for successive laser pulses and are therefore crucial for the local heat accumulation. The temporal PPD in primary scanning direction x is $\Delta t_x = f_p^{-1}$ and depends solely on pulse frequency, while the time difference in y depends on scan length and scanning velocity. For a unidirectional scanning strategy this time difference is $\Delta t_y = l_{\text{track}} \cdot v_{\text{scan}}^{-1}$ and for most cases $\Delta t_x \ll \Delta t_y$ is true (exceptions exist close to reversal points of a zigzag or meandering scanning pattern).

In most studies pulse frequencies up to $f_p = 40$ kHz are used for pulse durations in the nanosecond or microsecond regime. Temmler et al. [35] use for L μ P comparatively intermediate repetition rates of $f_p = 20$ kHz and pulse durations in the range of several hundred nanoseconds. The same repetition rate is also used by Pfefferkorn et al. [38] for successful laser polishing of S7 tool steel at pulse durations in the microsecond range. The temporal PPD is therefore usually not smaller than $dt = 25$ to $50 \mu\text{s}$ and is thus a central motivation to investigate pulse frequencies of up to 240 kHz and temporal PPD down to $4.16 \mu\text{s}$. Table 3 gives an overview of some relevant process parameters concerning pulse overlap and remelting cycles and their range.

In total, the number of remeltings is investigated in the range of approx. 7.2 times up to 85.9 times. Depending on the pulse frequency used, the temporal pulse-to-pulse distance (PPD) is between $3.125 \mu\text{s}$ and $50 \mu\text{s}$, while the spatial PPD is between $3.125 \mu\text{m}$ and $50 \mu\text{m}$. Accordingly, the pulse overlap is between 47.4% and 95.6%.

¹¹Nüsser [2] investigated the influence of the track overlap in the range of $dy = 22.5$ to $180 \mu\text{m}$ and found on the one hand that the influence of the pulse overlap on the required laser polishing fluence was higher than that of the track offset and justified this with the locally significantly different heat accumulation. On the other hand, he also came to the conclusion that an increase in the track offset led to less smoothing of the micro-roughness. The reason for this was presumably the more frequent remelting of the surface. As a result, surface defects caused by previous remelting processes are significantly smoothed again. The investigations by Nüsser [2] on the influence of the number of passes ($v_{\text{scan}} = 1500$ mm/s, $f_p = 20$ kHz, $dy = 45 \mu\text{m}$) on the roughness led to the conclusion that this depended significantly on the process gas atmosphere and the proportion of residual oxygen contained therein. Overall, the recommendation was to use a residual oxygen content at which the use of a single L μ P step led to the most homogeneous polishing result.

Table 3
Overview of remeltings depending on laser beam diameter, pulse frequency, scanning velocity and track offset.

Laser beam diameter d_L [μm]	Pulse frequency f_p [kHz]	Scanning velocity v_{scan} [mm/s]	Pulse-pulse-distance dx [μm]	Track offset dy [μm]	Remeltings n_x	Remeltings n_y
120	20	1000	50	25	1.9	3.8
120	80	1000	12.5	25	7.6	3.8
120	160	1000	6.25	25	15.1	3.8
120	240	1000	3.125	25	22.6	3.8
120	40	1000	25	25	3.8	3.8
140	40	1000	25	25	4.4	4.4
160	40	1000	25	25	5.0	5.0
200	40	1000	25	25	6.3	6.3

2.6.4. Process atmosphere

In a number of publications, L μ P is performed both in air and within a process gas atmosphere. The conduction of experiments within a defined process gas atmosphere should prevent unwanted or uncontrolled chemical reactions of the molten metal with the surrounding atmosphere, e.g. especially with oxygen. During L μ P of the titanium alloy Ti6Al4V without using a shielding gas atmosphere, Perry [11] reports that a thin surface layer with a high tendency to crack is formed. In comparison to that, Perry [11] reports further that no cracks appear when laser polishing in an argon atmosphere. Similar results were found by Yermachenko et al. [39], who observed a strong tendency for cracks while remelting the titanium alloy Ti3Al5Mo5V in a standard air atmosphere without a shielding gas. For the same titanium alloy, they

also observed that crack formation could be avoided by using a process atmosphere mainly consisting of the inert gas Argon. However, Li et al. [40] report that, during their experiments with single laser pulses on TiAl6V4, an additional oxide layer was formed that had a smoothing effect on the surface topography. This was also observed by Temmler et al. [6] during their investigations of areal L μ P, using a process gas atmosphere containing argon and a special residual oxygen content of 5000 ppm. Temmler [4] investigated the influence of the depth-dependent chemical element composition on material properties after laser polishing of hot work steel 1.2343 (AISI H11). Depending on the process parameters and the surrounding process gas atmosphere, the remelting process leads to a redistribution of the alloying elements within the remelted surface layer. At the boundary zone between remelted and heat-affected material, a change in the chemical composition is observed, which is particularly pronounced for the carbon content. During laser polishing, the process gas atmosphere has a significant influence on the chemical composition of the remelted surface layer and thus, among other things, on the formation of martensite, hardness and surface roughness. Nüsser [2] explicitly demonstrates that the process atmosphere significantly influences the roughness of Ti6Al4V samples after L μ P. The type of process gas, in particular, has a major influence on the surface topography. Nüsser [2] comes to the conclusion that the minimal roughness is achieved by using an oxygen content of $c(\text{O}_2) = 10$ ppm (smallest oxygen content investigated) in a process chamber filled with an Argon atmosphere. However, the fluence required to achieve the minimal roughness is not dependent on the oxygen content.

Overall, the use of an inert gas as a process atmosphere with low oxygen content can be regarded as a necessary prerequisite for a

Table 4
Overview of relevant process parameters and range of variation.

Process parameter	symbol	Range	Description
Laser beam diameter (pulsed)	d_L	120 μm –200 μm	Laser beam diameter of the pulsed laser beam on the component
Scan speed	v_{scan}	500 mm/s–2000 mm/s	The speed at which the laser beams are guided over the component
Average laser power	$P_{L, \text{max}}$	35 W	Maximal laser power of the pulsed laser beam on the component
Pulse energy	E_p	0.05 mJ–1.2 mJ	Pulse energy of the pulsed laser radiation on the component
Pulse duration	t_p	10 ns–220 ns	Duration of a laser pulse
Pulse repetition frequency	f_p	20 kHz–240 kHz	Repetition rate of pulsed laser radiation
Waveform	WF	0–5	Preset form and length of laser pulses
Track offset	dy	25 μm	Distance between single tracks
Crossings	n	1	Count of identical repetitions

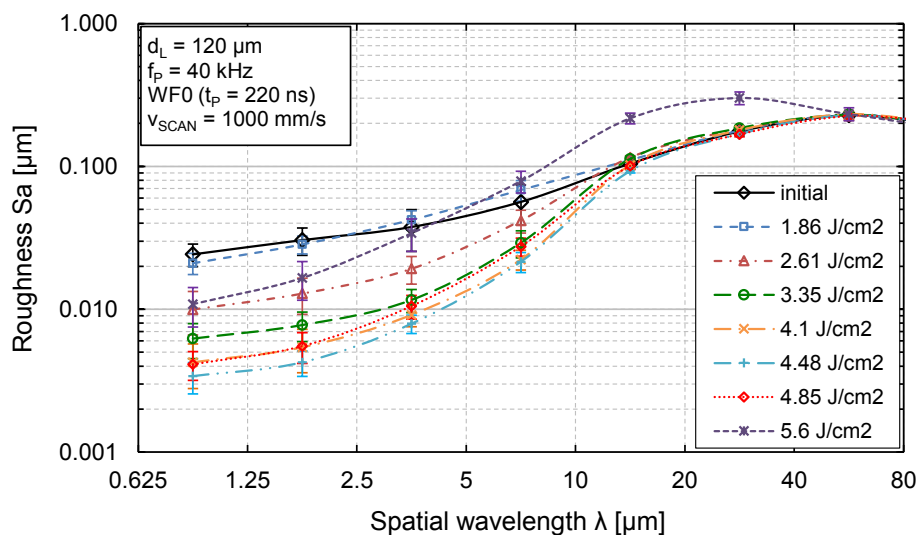


Fig. 14. Sa-spectrum for a variation of fluence at otherwise constant process parameters ($d_L = 120 \mu\text{m}$, WFO ($t_p = 220$ ns), $f_p = 40$ kHz, $v_{\text{scan}} = 1000$ mm/s, $dy = 25 \mu\text{m}$).

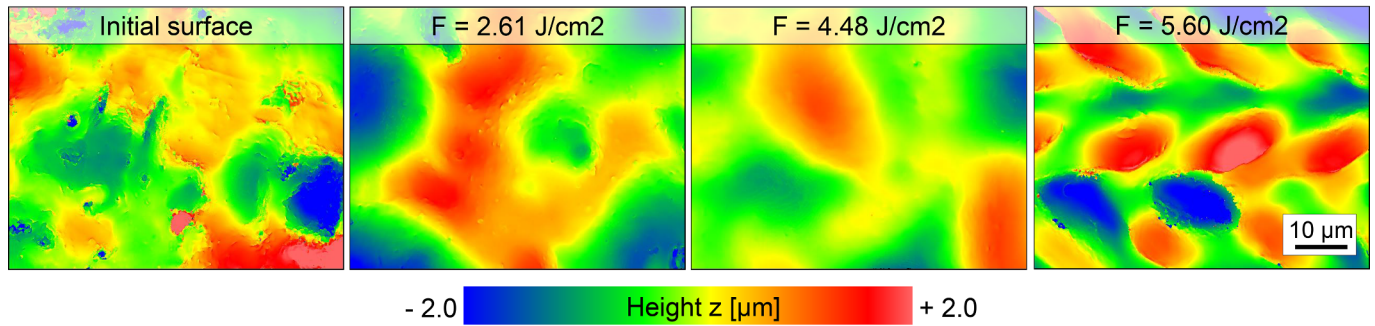


Fig. 15. Representative WLI images for LμP using different fluences ($d_L = 120 \mu\text{m}$; $f_p = 40 \text{ kHz}$; WFO; $t_p = 220 \text{ ns}$; $v_{\text{scan}} = 1000 \text{ mm/s}$; $dy = 25 \mu\text{m}$).

significant smoothing of the surface without simultaneous oxidation of the surface layer. Within this investigation Argon was used as an inert gas and the residual oxygen content was kept constantly below 100 ppm.

2.6.5. Overview of parameter range

Table 4 provides an overview, a brief description of the process parameters and the extent to which they are investigated within this work.

3. Results and discussion

3.1. Laser beam diameter

In order to determine an appropriate laser beam diameter for this investigation the laser beam diameter was varied in the range of $d_L = 120 \mu\text{m}$ up to $d_L = 200 \mu\text{m}$. This range was selected based on the maximum laser power and pulse energy available. In order to determine the minimal roughness for each laser beam diameter, fluence was varied in fourteen discrete steps for each laser beam diameter. The variation of fluence was effectively carried out by varying the average laser power and thus pulse energy for each individual laser beam diameter. The resulting surface roughness was analyzed by a Sa-spectrum.

Fig. 14 shows the Sa-spectrum for a laser beam diameter of $d_L = 120 \mu\text{m}$ and constant process parameters ($f_p = 40 \text{ kHz}$; WFO; $t_p = 220 \text{ ns}$; $v_{\text{scan}} = 1000 \text{ mm/s}$). Overall, the Sa spectrum shows a standard dependence of surface roughness on fluence for stainless steel AISI 410 (X12Cr13). As is usual for LμP, the initial surface roughness is smoothed down to a critical wavelength in the micro-roughness regime for spatial wavelengths of $\lambda = 10\text{--}20 \mu\text{m}$. The higher the fluence used,

the larger is the smoothing until a minimum roughness is achieved for the laser polishing fluence $F_{\text{pol}} = 4.48 \text{ J/cm}^2$ (Fig. 15). For fluences higher than F_{pol} , a comparatively smaller smoothing is achieved. If a fluence significantly higher than F_{pol} is used, partial material removal takes place. The recoil pressure of the ablated material deforms the melt pool, which leads to characteristic surface structures in the meso-roughness range. In Fig. 15 this can be observed for a fluence of $F = 5.6 \text{ J/cm}^2$ especially in the spatial wavelength regimes $\lambda = 10\text{--}20 \mu\text{m}$ and $\lambda = 20\text{--}40 \mu\text{m}$. This results from the used track offset of $dy = 25 \mu\text{m}$ and the local pulse-to-pulse distance of $dx = 25 \mu\text{m}$.

WLI images are shown in Fig. 15 and it has to be stated explicitly that the steel material used for this investigation shows no defects or cracks after LμP (besides residues of the initial surface roughness if laser polishing parameters are not optimized). This is generally an indication that the material is of high chemical homogeneity and has only a few sulfidic and oxidic inclusions.

Similar investigations were also carried out for the laser beam diameters $d_L = 140 \mu\text{m}$, $160 \mu\text{m}$ and $200 \mu\text{m}$. After varying the fluence, corresponding Sa-spectra of the laser remelted surfaces were used to determine the laser polishing fluence, which leads to the smallest roughness in combination with the other process parameters (Fig. 16a).

A comparison between the different laser beam diameters leads to two essential results. Firstly, the laser beam diameter used has only a minor influence on the minimum achievable roughness. Secondly, the fluence required to achieve the minimum roughness decreases as the laser beam diameter increases. However, it must be added that the fluence of $F = 2.62 \text{ J/cm}^2$ was the maximum fluence available for a laser beam diameter of $d_L = 200 \mu\text{m}$.

In addition, however, a comparison of the smoothing behavior with

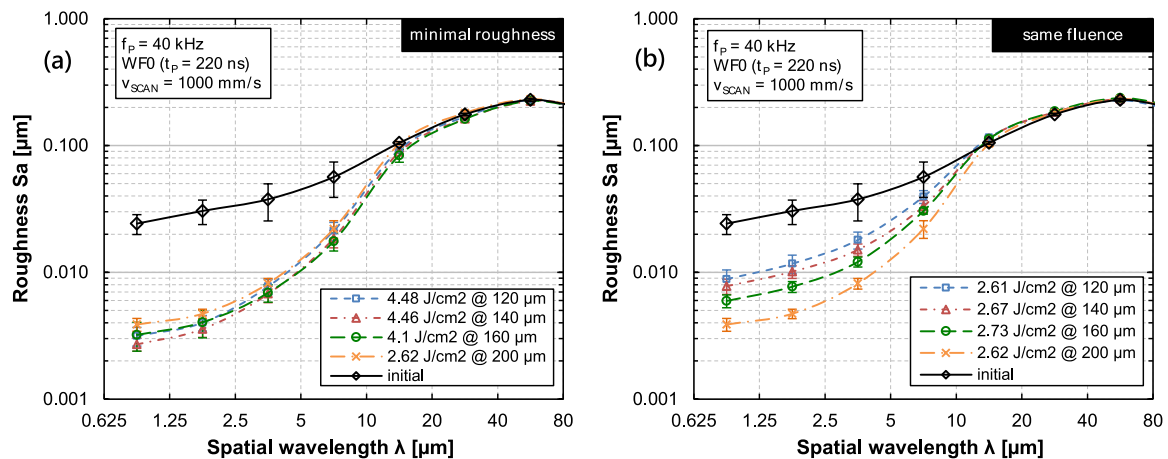


Fig. 16. Sa-spectra for laser polishing using different laser beam diameters. Sa-spectrum (a) compares the minimal roughness achieved with different laser beams. Sa spectrum (b) shows a comparison of spatial roughness for same fluence and different laser beam diameters at otherwise constant process parameters (WFO ($t_p = 220 \text{ ns}$), $f_p = 40 \text{ kHz}$; $v_{\text{scan}} = 1000 \text{ mm/s}$, $dy = 25 \mu\text{m}$).

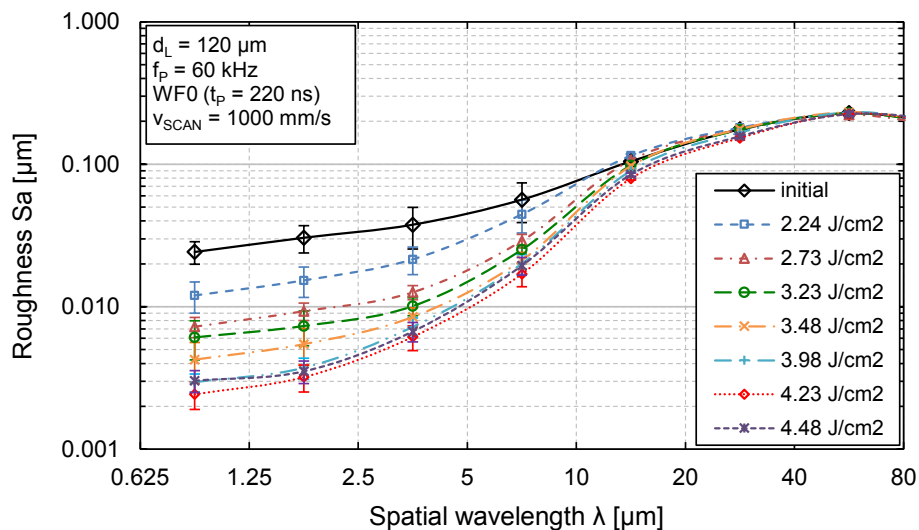


Fig. 17. Sa-spectrum for a variation of fluence at otherwise constant process parameters ($d_L = 120 \mu\text{m}$, WFO ($t_p = 220 \text{ ns}$), $f_p = 60 \text{ kHz}$, $v_{\text{scan}} = 1000 \text{ mm/s}$, $dy = 25 \mu\text{m}$).

almost the same fluence for the different laser beam diameters shows clear differences. The larger the laser beam diameter used, the smoother the roughness with otherwise identical process parameters. Since, in addition to the other process parameters, scanning speed and track offset are also constant, this leads to two possible explanations. On the one hand, an increasing laser beam diameter means that the overlap becomes larger with otherwise the same process parameters. This means that the surface is remelted more often and thus the amplitudes of the roughness could possibly be smoothed more. On the other hand, using the same fluence with different laser beam diameters means that the average laser power increases with the square of the radius as the laser beam diameter increases. Thus, more energy is absorbed by the surface boundary layer in the same time. The higher energy input per time might prolong the melt duration of the melt pool. The extension of the melt duration of the melt pool could in turn be attributed to a larger melt pool volume as well as to increased local heat accumulation by previous pulses. However, the temporal pulse-to-pulse distance is still $dt = 25 \mu\text{s}$, which is more than 100 times the pulse duration. Therefore, it seems that in this case the larger number of remeltings (from $n_x = n_y = 3.8$ for $d_L = 120 \mu\text{m}$ to $n_x = n_y = 6.3$ for $d_L = 200 \mu\text{m}$) has a larger influence on the reduction of surface roughness than the extension of the melt duration.

3.2. Pulse frequency (pulse duration: 220 ns)

Since the laser beam diameter has a comparatively small influence on the minimum achievable roughness, a laser beam diameter of $d_L = 120 \mu\text{m}$ is selected for further investigations. This also enables more room for variations in process parameters such as pulse duration and pulse frequency. Furthermore, the influence of the pulse frequency and thus the pulse overlap on the polishing result is investigated. The investigations for Waveform 0 ($t_p = 220 \text{ ns}$) are carried out at four different pulse frequencies ($f_p = 20, 40, 60, 80 \text{ kHz}$). Due to the change in pulse energy, temporal and spatial pulse-to-pulse distances are also changed (from $dx = 50 \mu\text{m}$ and $dt = 50 \mu\text{s}$ at 20 kHz to $dx = 12.5 \mu\text{m}$ and $dt = 12.5 \mu\text{s}$ at 80 kHz). This also implies that the surface is remelted four times more often with a pulse frequency of $f_p = 80 \text{ kHz}$ ($n_x = 7.6$) than for a pulse frequency of $f_p = 20 \text{ kHz}$ ($n_x = 1.9$), since scanning velocity is constant at $v_{\text{scan}} = 1000 \text{ mm/s}$.

Fig. 17 shows a Sa-spectrum of surfaces that were laser micro polished with a pulse frequency of $f_p = 60 \text{ kHz}$. The qualitative results correspond to those in Fig. 16. In comparison to a pulse frequency of $f_p = 40 \text{ kHz}$, the fluence, which leads to a minimum roughness, is

slightly smaller at $f_p = 60 \text{ kHz}$ with $F_{\text{pol}} = 4.23 \text{ J/cm}^2$. For the pulse frequencies $f_p = 20 \text{ kHz}$ and $f_p = 80 \text{ kHz}$, a variation of the fluence is also carried out with otherwise constant process parameters.

Fig. 18a shows the results for the minimum roughness achieved for the different pulse frequencies, where a fluence of $F = 3.36 \text{ J/cm}^2$ at $f_p = 80 \text{ kHz}$ is the maximum fluence available for this set of process parameters. Two basic tendencies can be identified. On the one hand, the laser polishing fluence F_{pol} decreases with increasing frequency. On the other hand, a smaller minimum roughness is achieved at higher pulse frequencies. Fig. 18b shows that with the same fluence, the smallest roughness is achieved at the highest pulse frequency. This is probably due to the smaller local and temporal pulse-to-pulse distance, which leads to an increase in local heat accumulation and thus to a longer melting time of the melt pool as well as to a more frequently remelted surface.

Fig. 18a also shows that a minimal roughness is achieved for almost the same fluence at pulse frequencies from $f_p = 20\text{--}60 \text{ kHz}$. This leads to the conclusion that the surface roughness is not smoothed more effectively due to local heat accumulation. Therefore, a higher number of remeltings, rather than a prolonged melt duration, is the cause of a smaller surface roughness. Since the laser polishing fluence is already reduced by approx. 5% for a pulse frequency of $f_p = 60 \text{ kHz}$ in comparison to 4.48 J/cm^2 at $f_p = 40 \text{ kHz}$, it is concluded that the surface needs to be remelted approx. 20 times ($n_x = 5\text{--}6$, $n_y = 3.8$) in order to achieve the minimal surface roughness.

3.3. Pulse duration and waveform

The influence of the pulse duration on the laser polishing results is investigated for the preset waveforms 0–5 with pulse durations in the range from 10 ns to 220 ns (Table 2). This is done by varying the fluence at a pulse frequency of $f_p = 80 \text{ kHz}$ and otherwise constant process parameters of $d_L = 120 \mu\text{m}$, $v_{\text{scan}} = 1000 \text{ mm/s}$, $dy = 25 \mu\text{m}$. The selected pulse frequency of $f_p = 80 \text{ kHz}$ represents a compromise between the selected laser beam diameter and the available maximum pulse energies for all pulse shapes and durations. Furthermore, this also guarantees that temporal and spatial PPD are the same for all test fields ($dx = 12.5 \mu\text{m}$ and $dt = 12.5 \mu\text{s}$) and the number of remeltings exceeds 20 times ($n_x \cdot n_y = 28.7$).

With a pulse duration of 220 ns , a significant smoothing but no material removal occurs at the maximum fluence (Fig. 19a). This changes with shorter pulse durations. At a pulse duration of 130 ns , the first material ablation takes place at a fluence of $F = 2.83 \text{ J/cm}^2$ and is

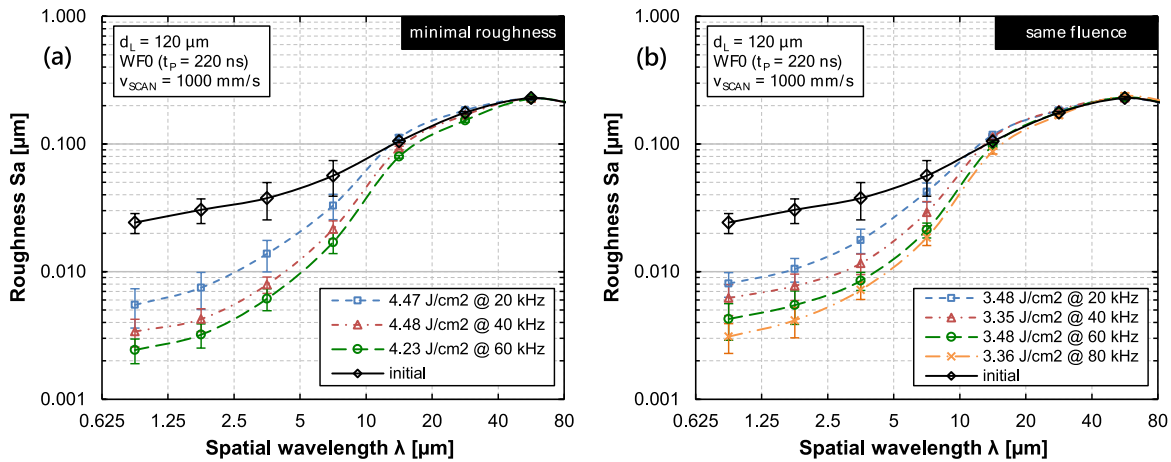


Fig. 18. Sa-spectra for minimal roughness (a) and the same fluence (b) $F = 3.41 \pm 0.07 \text{ J/cm}^2$ at different pulse frequencies $f_p = 20\text{--}80 \text{ kHz}$ ($d_l = 120 \text{ }\mu\text{m}$, WFO, $v_{\text{scan}} = 1000 \text{ mm/s}$, $d_y = 25 \text{ }\mu\text{m}$).

also evident from periodic ablation structures at $F = 3.24 \text{ J/cm}^2$ in the Sa-spectrum (Fig. 19b). With even shorter pulse durations of $t_p = 60 \text{ ns}$ (Fig. 19c), significant material removal already occurs at $F = 2.43 \text{ J/cm}^2$, which is noticeable in the Sa spectrum with a peak at 12.5 and 25 μm . For waveform 3 and $t_p = 30 \text{ ns}$ only a maximal fluence of $F = 2.01 \text{ J/cm}^2$ is available. At this fluence no material is ablated and the smallest roughness is achieved for a fluence of $F = 1.79 \text{ J/cm}^2$ (Fig. 19d).

For waveforms with even shorter pulse durations, namely waveform 4 and 5, only much smaller pulse energies and thus fluences up to $F = 1.17 \text{ J/cm}^2$ and 1.27 J/cm^2 , respectively, are available. This results from the fact that the PRF₀ frequencies of $f_p = 240 \text{ kHz}$ and 250 kHz are much higher than the pulse frequency used for the experiments (see also Table 2). Even with the highest pulse energies or fluences available at $f_p = 80 \text{ kHz}$, no material removal is observed when using waveform 4 (Fig. 19e) and waveform 5 (Fig. 19f). In addition, the roughness is smoothed only slightly. L μ P with the maximum pulse energy for the fluences $F = 1.17 \text{ J/cm}^2$ and 1.27 J/cm^2 , respectively, in combination with the short pulse durations, only smooths the micro-roughness by max. 50% for spatial wavelengths $\lambda \ll 5 \text{ }\mu\text{m}$.

A comparison of the roughness achieved with the same fluence seems to lead to the result that the roughness is smoothed all the more the longer the pulse duration used is (Fig. 20b). However, the result of this comparison depends very much on the selected fluence. At a fluence of $F = 1.62 \text{ mJ/cm}^2$ the greatest smoothing of the roughness is achieved at a pulse duration of 30 ns or 60 ns (Fig. 20a).

On the one hand, one reason might be the increased peak pulse power for shorter pulse durations. In this case, melting and smoothing of the surface would already occur at lower fluences. On the other hand, the significant dispersion of the roughness for the two longer pulse durations of $t_p = 130 \text{ ns}$ and $t_p = 220 \text{ ns}$ shows a comparatively inhomogeneous smoothing of the roughness. Thus, the dispersion of roughness from the initial roughness has a significant influence on the roughness achieved in the micro range. This applies in particular to fluences that are significantly smaller than the laser polishing fluence. Therefore, a comparison of the minimum roughness achieved with the respective pulse durations seems to be the most meaningful.

For this comparison, Fig. 21 shows a clear result. For an otherwise constant set of process parameters, the minimum roughness is achieved with the longest pulse duration. Generally speaking, the longer the pulse duration used, the smaller the minimal roughness and the longer the critical spatial wavelength become. However, for spatial wavelengths $\lambda < 1.25 \text{ }\mu\text{m}$, the same micro-roughness is achieved for all the pulse durations investigated. Furthermore, the laser polishing fluence F_{pol} at which the minimum roughness is achieved becomes smaller with shorter pulse durations. Presumably, this results from an increased

pulse peak power for the same fluence at shorter pulse durations, which lowers the ablation threshold (pulse energy) for shorter pulse durations.

3.4. L μ P with pulse frequencies $f_p \geq 160 \text{ kHz}$ and characteristic of the remelting process

The combination of pulse energy and pulse frequency for waveforms 4 and 5 is not yet sufficient to achieve an effective smoothing of the surface. Therefore, further investigations of these waveforms are carried out at significantly higher pulse frequencies and, correspondingly, lower temporal and spatial PPD. To ensure that not only the maximum available pulse energy but also the maximum average laser power is used for each waveform, the investigations are performed close to the respective PRF₀ frequencies. For waveform 3 the investigations are therefore performed at a pulse frequency of 160 kHz, for waveform 4 and waveform 5 at a pulse frequency of 240 kHz. The available maximum pulse energies and laser powers can be taken from Table 2.

For all pulse durations, a significant reduction in micro-roughness is achieved by increasing the pulse frequency to $f_p = 160 \text{ kHz}$ for waveform 3 (Fig. 22a) and to $f_p = 240 \text{ kHz}$ for waveform 4 (Fig. 22b) and waveform 5 (Fig. 22c). The comparison of the minimal roughness in Fig. 22d shows that an increase of pulse frequency close to the PRF₀ frequency in combination with an adaption of fluence lead to a similar reduction in roughness for pulse durations in the range of $t_p = 10\text{--}30 \text{ ns}$. Similarly, no significant difference in the critical wavelength among these pulse durations is visible. Therefore, it can be concluded that the melt duration of the melt pool is about the same. Furthermore, it can be seen that the laser polishing fluence $F_{\text{pol}} = 1.82 \text{ J/cm}^2$ for a pulse duration of $t_p = 30 \text{ ns}$ is significantly higher than for the two shorter pulse durations. Additionally, this laser polishing fluence is almost the same as for a pulse frequency of $f_p = 80 \text{ kHz}$ (Fig. 21). This leads to the conclusion that **the larger number of remelting cycles, rather than the local heat accumulation, is predominantly responsible for the lower roughness.**

Although the available fluence at waveform 0 for $f_p = 80 \text{ kHz}$ is not sufficient to achieve a maximal smoothing (Fig. 19a), the pulse frequency is further doubled to $f_p = 160 \text{ kHz}$ ($dt = 6.25 \text{ }\mu\text{s}$) and scan speed is halved to $v_{\text{scan}} = 500 \text{ mm/s}$ in order to take advantage of local heat accumulation if possible. Since pulse frequency is doubled and scan speed is halved, temporal PPD is quartered. The spatial PPD is halved at the same time.

Fig. 23a shows that the minimal roughness is achieved for a laser polishing fluence of $F = 1.42 \text{ J/cm}^2$. Compared to L μ P at $f_p = 80 \text{ kHz}$, a significantly lower fluence F_{pol} is required to achieve approximately the same smoothing of surface roughness (Fig. 23b). The fluence is only about one third of the laser polishing fluence at $f_p = 80 \text{ kHz}$. In this

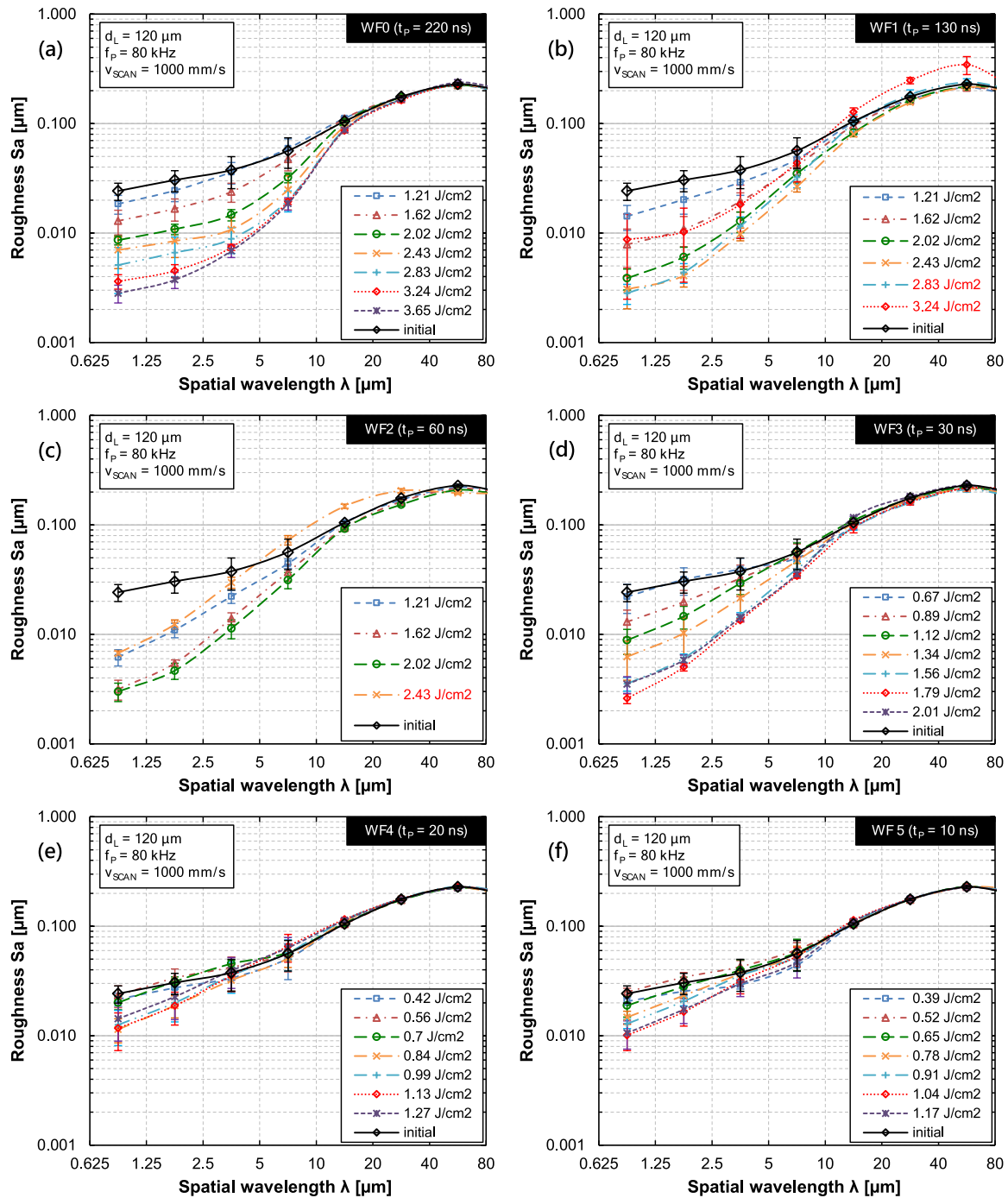


Fig. 19. Sa-spectra for laser polished surfaces at different waveforms, pulse durations and fluences. (a) Waveform 0 and $t_p = 220$ ns, (b) Waveform 1 and $t_p = 130$ ns, (c) Waveform 2 and $t_p = 60$ ns, (d) Waveform 3 and $t_p = 30$ ns, (e) Waveform 4 and $t_p = 20$ ns, (f) Waveform 5 and $t_p = 10$ ns. ($d_L = 120$ μm , $f_p = 80$ kHz, $v_{\text{scan}} = 1000$ mm/s, $d_y = 25$ μm).

range of process parameters, the smaller temporal PPD and spatial PPD seem to have a significant influence on the local heat accumulation and thus on the required fluence. Furthermore, at $f_p = 160$ kHz, the roughness in the local wavelength range of $\lambda = 10\text{--}20$ μm is also significantly smoother. This, in turn, is usually accompanied by a significant increase in the melt duration of the molten material in the melt pool. However, in contrast to the usual behavior, the roughness then stays almost constant at the minimum roughness. An examination of WLI images for the fluences in the range of $F = 1.21\text{--}1.82$ J/cm² shows a significant change in the characteristic of the surface topography, although the micro-roughness in particular keeps almost constant at a low roughness level (Fig. 24).

For the laser polishing fluence of $F_{\text{pol}} = 1.42$ J/cm² no surface structures are visible other than the smoothed initial structure. For an increase of fluence to $F = 1.62$ J/cm², additional ripple like structures are visible all over the surface, which is an indicator for local evaporation of material due to vapor pressure (and/or thermocapillary flow). However, a further increase of fluence to $F = 1.82$ J/cm² does not lead to deeper and more defined structures that are residues of single pulses, but distinctive horizontal lines are clearly visible that show almost no rippling. The distance between these horizontal lines is approx. 25 μm , which equals the track offset used for laser polishing. The formation of these homogenous melting tracks without crater-like indentations and clearly visible border lines in the distance of the

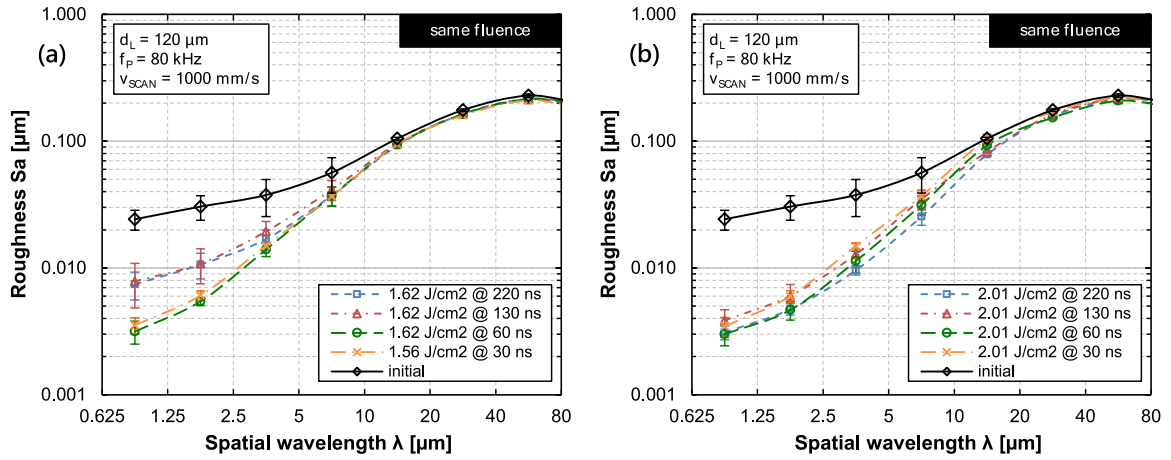


Fig. 20. Sa-spectra of laser polished surfaces for two different fluences $F = 1.62 \text{ J/cm}^2$ (a) and $F = 2.01 \text{ J/cm}^2$ (b). ($d_L = 120 \mu\text{m}$, $f_p = 80 \text{ kHz}$, $v_{\text{scan}} = 1000 \text{ mm/s}$, $dy = 25 \mu\text{m}$).

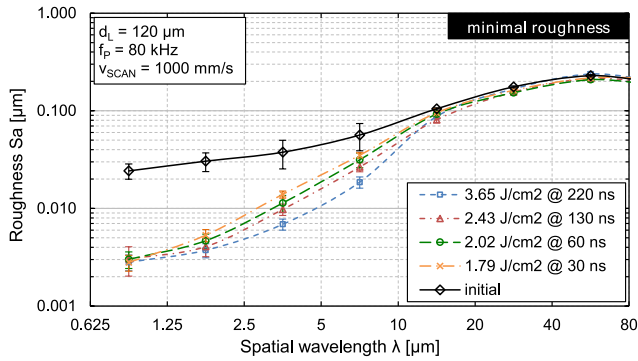


Fig. 21. Sa-spectrum for minimal roughness achieved with waveforms WF0 to WF3 and according pulse durations from $t_p = 220 \text{ ns}$ – 30 ns . ($d_L = 120 \mu\text{m}$, $f_p = 80 \text{ kHz}$, $v_{\text{scan}} = 1000 \text{ mm/s}$, $dy = 25 \mu\text{m}$).

track offset are strong indicators that a continuous melt pool was formed. Without high-speed imaging or extensive theoretical calculations, it is difficult to resolve whether a discrete or continuous remelting process is responsible for this kind of difference in surface structure. Therefore, an approximation is derived, among others, based on melt durations and the principle of heat accumulation reported in other publications.

In principle, a continuous remelting process takes place when the melt duration t_{melt} of the melt pool exceeds the time interval between successive laser pulses f_p^{-1} .

$$t_{\text{melt}} \geq \frac{1}{f_p} \quad (5.1)$$

In this case, the ratio of temporal PPD to pulse duration is approximately 28.5 to 1 ($f_p^{-1} = 6.25 \mu\text{s}$ to $t_p = 0.22 \mu\text{s}$ —if pulse duration equals melt duration). Thus, the criterion for a continuous remelting process does not seem to be fulfilled. However, it should be noted that the interaction zone of laser radiation and material surface is irradiated several times by laser pulses and thus a significant heat accumulation can be assumed [41]. Weber et al. [42] introduced the “heat accumulation equation” for pulsed laser processing. Although the basic assumption that the pulse energy is applied in an infinitesimal, short time and volume does not hold for the micro laser polishing process, the key physical effect of heat accumulation is assumed to be very similar. In contrast to Weber et al. [42], for the present case of L μ P, we assume that heat accumulation and pulse duration are in the range of nanoseconds to microseconds. The basic assumption for a quasi-continuous remelting process is that heat accumulation leads to a heating temperature greater than the melting temperature of the material

($T_{\text{heat}} > T_{\text{melt}}$). At the same time the maximum process temperature should not exceed the evaporation temperature of the material ($T_{\text{max}} < T_{\text{vap}}$). Furthermore, a remelting process with cw laser radiation can be seen as a pulsed laser process with infinite pulse frequency ($f_p \rightarrow \infty$). Heat accumulation for very high frequencies should therefore lead to a heating temperature that equals the process temperature for a cw process at given average laser power ($T_{\text{heat}} = T_{\text{process,cw}}$). Another limitation for the quasi-continuous remelting process exists for the maximum pulse energy. The maximum pulse energy should not lead to an increase in temperature that is greater than the difference of evaporation temperature and melting temperature ($\Delta T_{\text{max}}(E_{p,\text{max}}) < T_{\text{vap}} - T_{\text{melt}}$)¹².

The melt duration depends on fluence, heat accumulation, pulse duration, and the characteristic material properties¹³. In the present case, heat accumulation is estimated according to the number of remelting cycles per area. The interaction time between surface and laser radiation is estimated by the quotient of laser beam diameter and scan speed ($t_{\text{int}} = d_L \cdot v_{\text{scan}}^{-1}$). The number of laser pulses interacting with the surface during this time is thus $n_p = t_{\text{int}} \cdot f_p = d_L \cdot v_{\text{scan}}^{-1} \cdot f_p$. This takes account of the fact that both smaller temporal and spatial PPD lead to an increased heat accumulation. An effective pulse duration within this interaction time is estimated with the product of $t_{p,\text{eff}} = n_p \cdot t_p = 8.45 \mu\text{s}$, and is already longer than the temporal PPD of $dt = 6.25 \mu\text{s}$. The assumption that the effective pulse duration equals the melt duration at L μ P conditions results in $t_{\text{melt}} = t_{p,\text{eff}}$ ¹⁴. This leads to the following criterion for a ‘critical’ scanning velocity, below which the discrete, pulsed L μ P process presumably changes to a continuous remelting process:

$$v_{\text{scan}} \leq d_L \cdot t_p \cdot f_p^2; \text{ with } t_{p,\text{max}} \leq \frac{1}{2} \cdot f_p^{-1} \quad (5.2)$$

¹² It has to be noted that existence and value of this pulse energy depends also significantly on differences in absorption coefficients for laser radiation in the solid and the molten phase of the material. If the absorption coefficient of the molten phase increases significantly in comparison to the solid phase, this would result in a significantly smaller maximum pulse energy. A consequence could be that this pulse energy is not sufficient to melt the material.

¹³ Nüsser [2] conducted simulations based on $1.28 \mu\text{s}$ pulses and fluences between 3.73 and 7.68 J/cm^2 using Ti6Al4V. The melt duration depends approximately linearly on the fluence and thus pulse energy. In contrast to other theoretical work, a local heat accumulation of 4 pulses, i.e. a pulse overlap of approx. 80%, was taken into account.

¹⁴ L μ P-conditions mean that a material-adapted laser polishing fluence F_{pol} exists that leads to a reduction of surface roughness of this specific material. Furthermore, it means that a fluence close to the laser polishing fluence was chosen for the L μ P process.

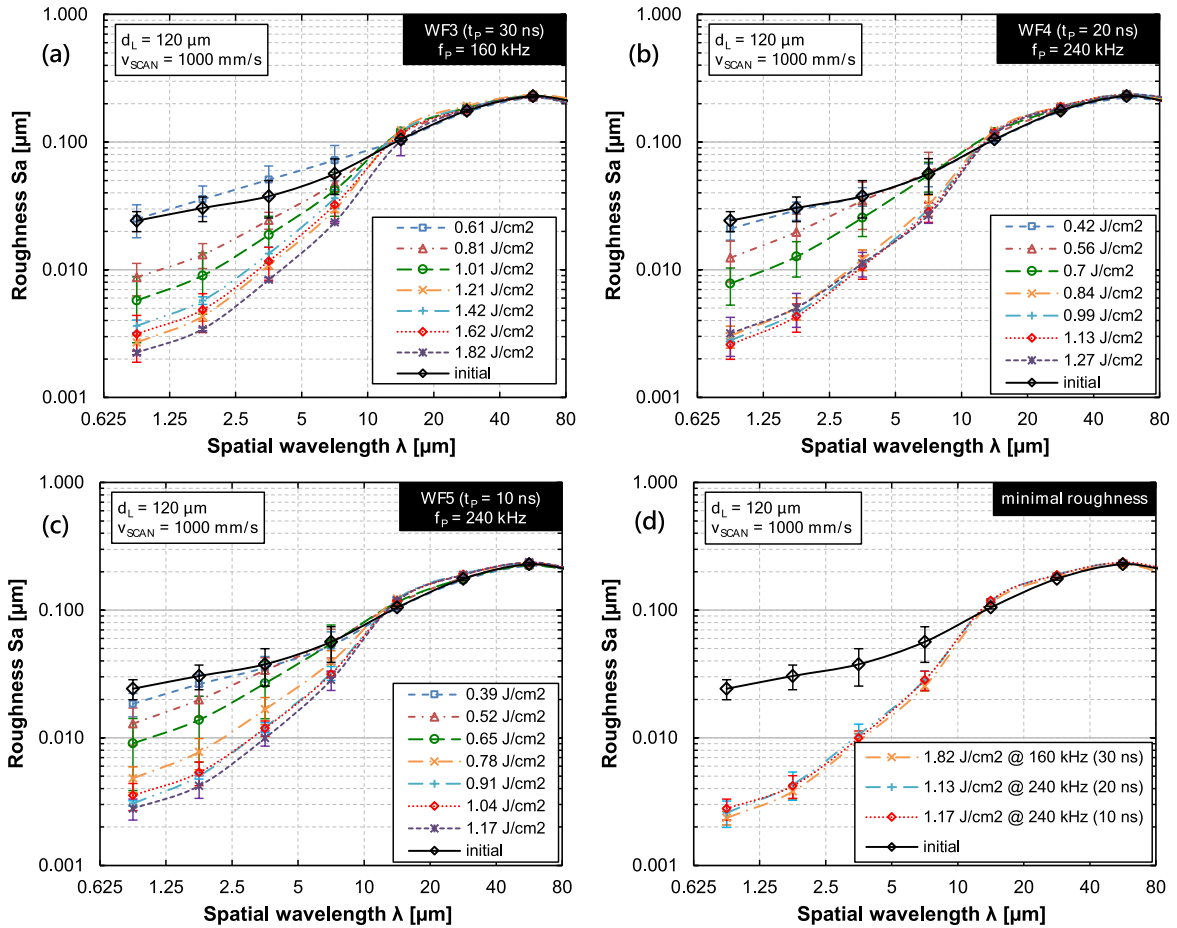


Fig. 22. Sa-spectra for $L_{\mu}P$ with waveforms 3 (a), 4 (b) and 5 (c) for a variation of fluence; Sa-spectrum for the minimal achieved roughness for waveforms 3, 4 and 5 (d). ($d_L = 120 \mu\text{m}$, $v_{\text{SCAN}} = 1000 \text{ mm/s}$, $d_y = 25 \mu\text{m}$).

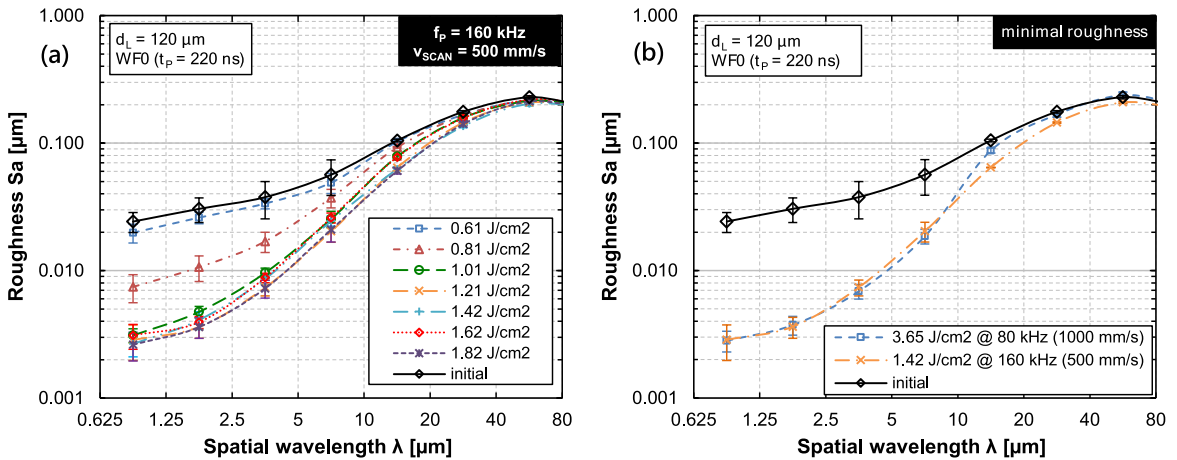


Fig. 23. Sa-spectrum for a variation fluence for WF0 at $f_p = 160 \text{ kHz}$ and $v_{\text{SCAN}} = 500 \text{ mm/s}$ (a) and for the minimal roughness achieved at different pulse frequencies (b) ($d_L = 120 \mu\text{m}$, WF0 ($t_p = 220 \text{ ns}$), $f_p = 80/160 \text{ kHz}$, $v_{\text{SCAN}} = 1000 \text{ mm/s} / 500 \text{ mm/s}$, $d_y = 25 \mu\text{m}$).

If the scanning speed on the left side of Eq. (5.2) is smaller than the right side, it is more likely to be a continuous remelting process than a discrete, pulsed $L_{\mu}P$ process. This empirical estimate leads to the result that a continuous remelting process is to be expected for scanning velocities of less than approx. 675 mm/s, if fluences are used that are close to the laser polishing fluence (at $d_L = 120 \mu\text{m}$, $t_p = 220 \text{ ns}$ and $f_p = 160 \text{ kHz}$). At the same time, it holds for the other results of this study. For example it supports the observation that, at pulse frequencies of $f_p = 160 \text{ kHz}$ or 240 kHz and pulse durations of 30 ns or 20 ns at

$v_{\text{SCAN}} = 1000 \text{ mm/s}$, no indications for a continuous remelting process have been observed. Using Eq. (5.2) for these cases, the 'critical' velocities would therefore be approximately 185 mm/s and 276 mm/s, respectively.

For examples from literature, e.g. Hafiz et al. [22] with a pulse frequency in the megahertz range ($t_p = 10.5 \text{ ps}$, $f_p = 7.45 \text{ MHz}$, $d_L = 35 \mu\text{m}$, $P_L = 12 \text{ W}$, $v_{\text{SCAN}} = 20 \text{ mm/s}$, $F = 0.19 \text{ J/cm}^2$), this 'critical' scanning velocity would be calculated to be approx. 20.4 mm/s. This result would suggest that this could be a continuous remelting

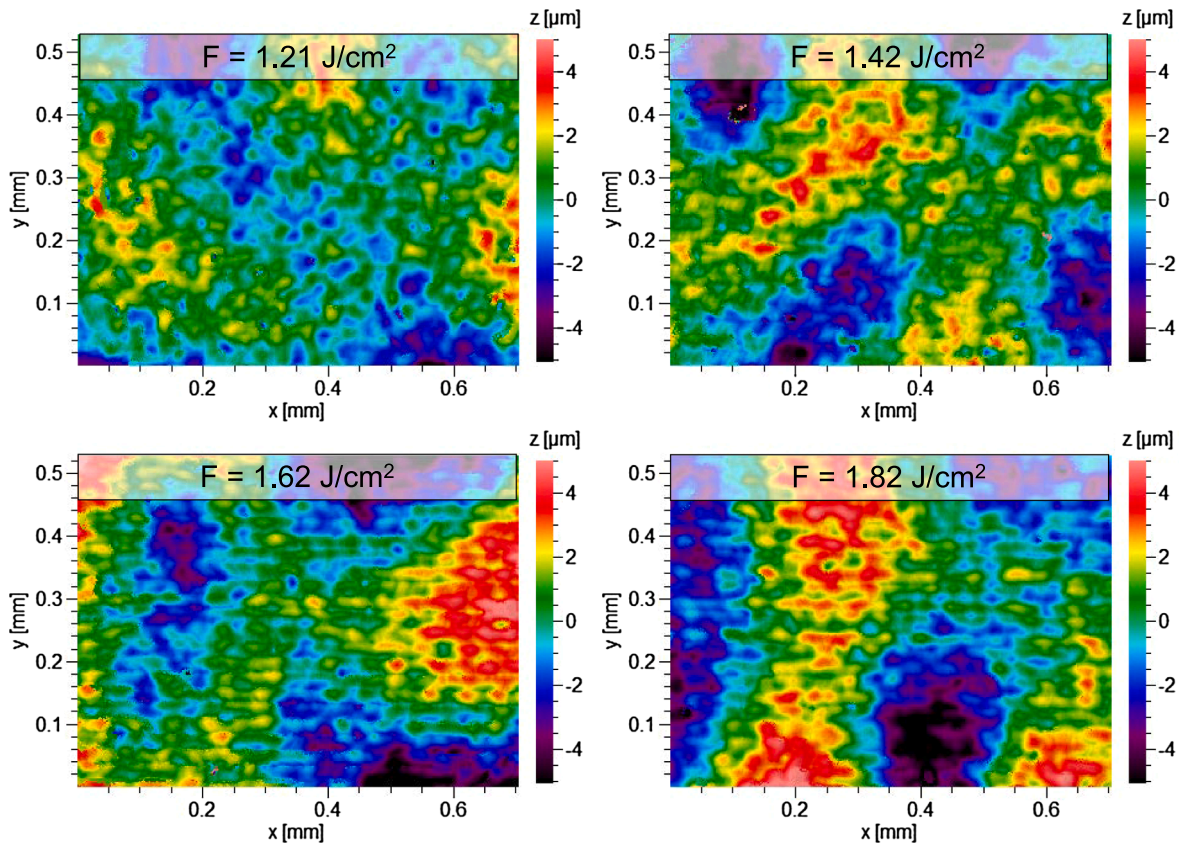


Fig. 24. WLI images of laser polished surfaces with different fluences from $F = 1.21 \text{ J/cm}^2$ to $F = 1.82 \text{ J/cm}^2$. ($d_L = 120 \text{ }\mu\text{m}$, WFO ($t_p = 220 \text{ ns}$), $f_p = 160 \text{ kHz}$, $v_{scan} = 500 \text{ mm/s}$, $dy = 25 \text{ }\mu\text{m}$).

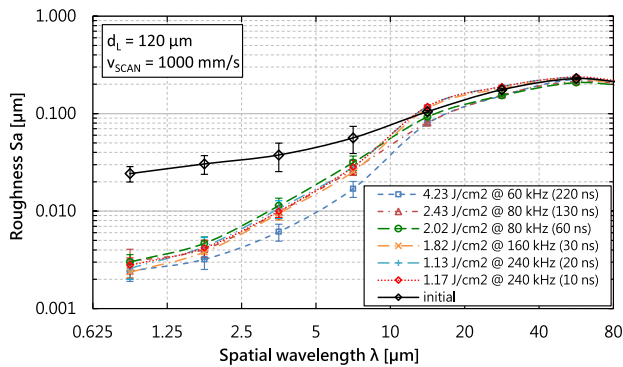


Fig. 25. Sa-spectrum for the minimal roughness achieved with different waveforms, fluences and pulse frequencies ($d_L = 120 \text{ }\mu\text{m}$, $v_{scan} = 1000 \text{ mm/s}$, $dy = 25 \text{ }\mu\text{m}$).

process or a discrete L μ P process. Process parameters ($t_p = 1.28 \text{ }\mu\text{s}$, $f_p = 20 \text{ kHz}$, $d_L = 375 \text{ }\mu\text{m}$, $v_{scan} = 1500 \text{ mm/s}$, $F = 4.55 \text{ J/cm}^2$) often used by Nüsser [2] would result in a 'critical' scanning velocity of approx. 384 mm/s. This 'critical' scanning velocity indicates a discrete process. For process parameters used by Pfefferkorn et al. [38] ($t_p = 5.6 \text{ }\mu\text{s}$, $f_p = 20 \text{ kHz}$, $d_L = 85 \text{ }\mu\text{m}$, $P_{L, peak} = 30 \text{ W}$, $v_{scan} = 100\text{--}1600 \text{ mm/s}$), it can be assumed, using Eq. (5.2), that a scanning velocity smaller than $v_{scan} = 190 \text{ mm/s}$ is rather likely to result in a continuous remelting process. Furthermore, for these quasi-continuous remelting processes the formation of Marangoni flow is more likely than in a discrete remelting process. This might be a reason for different findings and hypotheses about the potential effect of Marangoni flow on surface roughness during L μ P.

In any case, it should be noted that Eq. (5.2) is an estimation based

on empirical experience rather than a precise calculation. Especially for fluences significantly larger than the laser polishing fluence, a higher 'critical' scanning velocity and partial material ablation can be expected. However, by considering key process parameters for L μ P such as laser beam diameter, pulse duration, pulse frequency and scanning velocity this might be a useful method to estimate whether the laser polishing process is more likely to have continuous or discrete remelting characteristics. In any case, further theoretical investigations need to be carried out in order to verify that a quasi-continuous remelting process exists, and, if it exists, for which process parameters this quasi-continuous process can be expected.

3.5. Comparison of minimal roughness

The minimum surface roughness achieved with different waveforms, i.e. pulse durations, is compared in Fig. 25. The smallest micro-roughness is achieved with the highest pulse duration, i.e. at WFO with $t_p = 220 \text{ ns}$, a pulse frequency of $f_p = 60 \text{ kHz}$ and a laser polishing fluence of $F_{pol.} = 4.23 \text{ J/cm}^2$. However, the greatest reduction of meso-roughness, especially for the range $\lambda = 10\text{--}20 \text{ }\mu\text{m}$, is achieved at $f_p = 160 \text{ kHz}$ and a laser polishing fluence of $F_{pol.} = 1.42 \text{ J/cm}^2$ (Fig. 23b).

The minimum roughness achieved with pulse durations in the range of $t_p = 10\text{--}130 \text{ ns}$ is approximately the same for all pulse durations. However, the achieved roughness is greater than for a pulse duration of $t_p = 220 \text{ ns}$. The laser polishing fluence becomes smaller with shorter pulse durations, since the same fluence at smaller pulse durations leads to higher pulse peak powers and thus to evaporation at smaller fluences. At the same time, for shorter pulse durations, the roughness is smoothed more effectively by using high pulse frequencies up to $f_p = 240 \text{ kHz}$. The reason is presumably an increased local heat accumulation that leads to an increase in the melt duration of the molten

material. Overall, a significant smoothing of the roughness is achieved without material removal for all pulse durations investigated. Furthermore, all results indicate that the process parameters used in this comparison are still within the boundaries of a discrete rather than a continuous remelting process.

3.6. Evaluation of surface quality and mechanical properties

Besides surface roughness, the influence of laser polishing on the thermo-mechanical properties of the remelted are complex and strongly dependent on the process parameters chosen for laser polishing. Temmler [4] states that the process parameters have a decisive influence on the local and temporal temperature gradients relevant for microstructure formation. Mechanical properties like hardness and corrosion resistance of surfaces are often significantly influenced by the size of microstructure and the distribution of chemical components at the near-surface region. Mai and Lim [27] report that laser surface remelting has been widely investigated and applied to improve wear and corrosion properties of different materials. The improvement is mainly due to the rapid melting and cooling, which modify the surface microstructure of the material. In this context, Preußner et al. [43] states that from a metallurgical point of view laser polishing, like welding, equals a local remelting and a heat treatment with rapid heating and cooling rates ($\sim 10^5$ – 10^7 K/s) that often results in a surface hardening (depending on the initial state). Detailed investigations on X90CrMoV18 and 100Cr6 of Liebing [44] show that the influence of hardness depends not only on the material but also strongly on the process parameters. Morrow et al. [45] find for the remelted surface layer of S7 tool steel that surface hardness after laser melting is between an annealed and a furnace hardened state, and that it strongly depends on the process parameters used (using nano-indentation micro-hardness measurements). For process parameters resulting in good laser polishing outcomes, the hardness is generally significantly closer to a furnace hardened state.

Besides exemplary surface hardness measurements, a detailed evaluation of mechanical properties is beyond the scope of this investigation. The results of surface hardness measurements for selected fields and process parameters show that there is almost no change in surface hardness in comparison to the initial state. Vickers hardness measurements (HV1) result in an average surface hardness of 323 (± 21) HV for the initial state, while the surface hardness for most L μ P fields stays almost the same at 335 (± 36) HV. There was one exception that could be measured for a special set of process parameters ($d_L = 120 \mu\text{m}$, WF0 ($t_p = 220 \text{ ns}$), $f_p = 160 \text{ kHz}$, $v_{\text{scan}} = 500 \text{ mm/s}$, $dy = 25 \mu\text{m}$, $F = 1.82 \text{ J/cm}^2$) that are expected to create a continuous rather than a discrete process. The hardness for this field was measured to be 409 (± 16) HV and is significant higher than for the initial material. A comparison of surface hardness for two laser fluences of $F = 1.21 \text{ J/cm}^2$ (331 HV) and $F = 1.82 \text{ J/cm}^2$ (409 HV) shows that an increased hardness is achieved for higher fluence. Moradi et al. [46] measured micro hardness as high as 762 HV for laser surface hardened AISI 410. Although one would expect that cooling and heating rates for their surface hardening process would be significant smaller than for L μ P. Therefore, in contradiction to our results, a higher surface hardness could be expected for L μ P. However, Willenborg [3] finds that the thickness of the remelted surface layer for L μ P is usually less than 5 μm . Since the imprint of the hardness measurement is deeper than 5 μm , it can be assumed that the remelted layer only has a small influence on the hardness measurement. However, this influence should increase if the thickness of the remelted layer increases. This means that the surface hardness presumably increases, if a thicker surface boundary layer is remelted. Therefore, it can be assumed that the surface hardness of the remelted surface layer is significantly higher than for the initial material, and that the remelted layer (presumably of a quasi-continuous process) is thicker than that for a discrete remelting process. Nevertheless, a further, detailed investigation into surface layer thickness

(e.g. based on cross-sections) and its micro-hardness (e.g. by nano-indentation) should be conducted in order to find some hard evidence for these hypotheses.

3.6.1. Surface defects and corrosion resistance

Surface defects are often visible on surfaces after L μ P if the quality of the material is low. These surface defects after L μ P are divided into the categories “craters” (narrow and deep) and “hollows” (wide and shallow) by Liebing [44] and are mainly caused by sulfidic (mostly MnS) and oxidic (mostly Al_2O_3) inclusions; nitrides have almost no influence on the formation of surface defects. Nüsser et al. [18] state that sulfidic inclusions like MnS (or their products of decomposition) usually have a higher absorption coefficient for laser radiation than the bulk material, while a low thermal conductivity usually leads to heat accumulation in oxidic inclusions. Hollows are not only formed by multiple remeltings of craters but can also be formed due to an intensity gradient within the laser beam [44]. Li et al. [40] report that in aluminum alloys (e.g. AlCu4MgSi), intermetallic phases may also cause surface defects. Overall, the number and size of surface defects depend significantly on the process parameters. However, they depend even more on the chemical composition of the material, the homogeneity of the distribution of the chemical elements and the number and size of oxidic and sulfidic inclusions. The corrosion resistance of laser micro polished surfaces depends on the material, on the process parameters (possible formation of a passivation layer) and, in particular, on the type, number and shape of surface defects. Morrow et al. [45] find micro-cracks with a length of less than one micrometer in the vicinity of the melt pool edges (S7 tool steel after L μ P). Furthermore, larger cracks were formed with a length of approximately ten micrometers. The final size of these cracks depends significantly on the residual stress state resulting from laser remelting of the material. Therefore, choosing the correct process parameters is not only crucial to achieve a minimal roughness but also plays a crucial role in preventing micro-cracks.

In contrast to the cited research work, formation of micro- or macro-cracks has not been observed after L μ P of AISI 410. The remelted surface is very homogenous and virtually free of surface defects or holes after L μ P. Therefore, it is assumed that the material is of high quality in terms of number and size of sulfidic or oxidic inclusions. In addition, this is also an indicator for a homogenous distribution of the chemical elements within the bulk material. Therefore, an increase in wear resistance and especially in corrosion resistance is very likely. This needs to be verified in future investigations. Furthermore, investigations on the influence of L μ P on the residual austenite content, residual stresses, wettability and wear properties are recommended in order to fully evaluate the changes in thermo-mechanical properties of AISI 410 after L μ P.

3.7. Application

In agreement with Chow et al. [12], L μ P of AISI 410 mainly reduces the micro-roughness of a metallic surface. The special characteristic of gloss enhancement, as has been reported by Temmler et al. [35] for AISI H11, is also clearly visible for L μ P of AISI 410. This makes it possible to specifically adjust the gloss level of surfaces by adjusting the surface roughness in this spatial wavelength interval from $\lambda = 0.625$ to 1.25 μm [47]. A physical parameter, closely related to the degree of gloss, is the directional reflection, which is also significantly increased by L μ P [27]. Fig. 26 shows a comparison of the initial surface and a laser polished surface, on which the lowest surface roughness was achieved, at two different magnifications. The smoothing of the surface in the micrometer range is clearly visible. Structures with spatial dimensions larger than approx. 50 μm stay virtually unaffected.

In addition to Fig. 7, these results show not only that a significant reduction of roughness was achieved, but also that a similar increase in gloss was achieved. This increase in gloss was utilized to create a dual gloss effect on a structured surface (Fig. 27). This surface was created

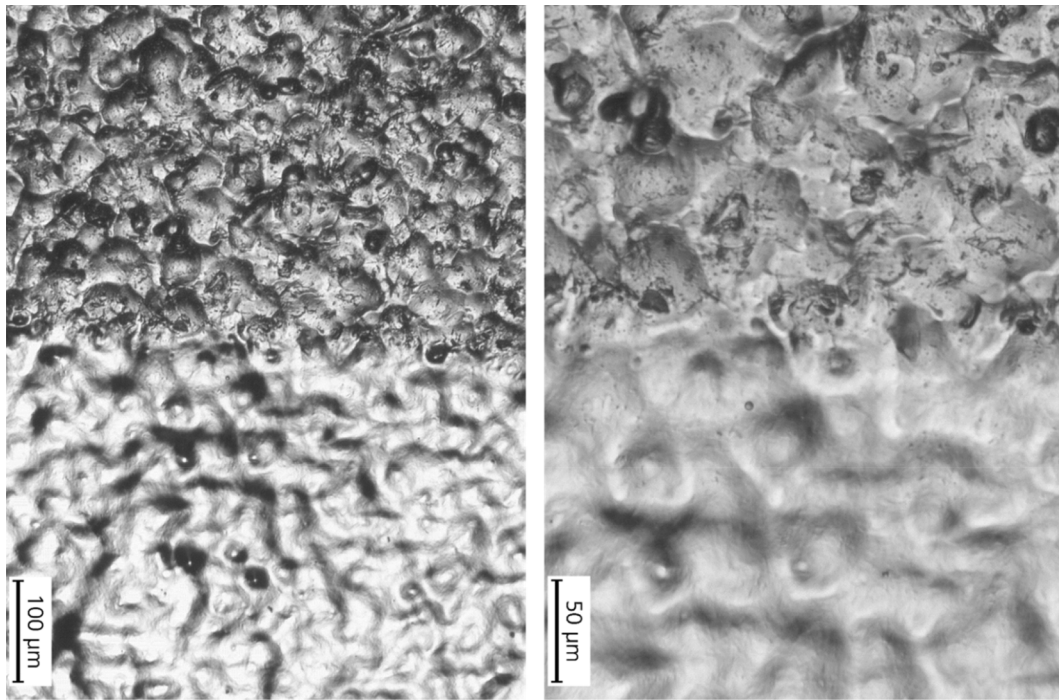


Fig. 26. Microscopic images in two different magnifications for the comparison of the initial surface and the laser polished surface, which has the minimal micro-roughness achieved within this study ($d_L = 120 \mu\text{m}$, WFO ($t_p = 220 \text{ ns}$), $f_p = 60 \text{ kHz}$, $v_{\text{scan}} = 1000 \text{ mm/s}$, $dy = 25 \mu\text{m}$, $F = 4.23 \text{ J/cm}^2$).

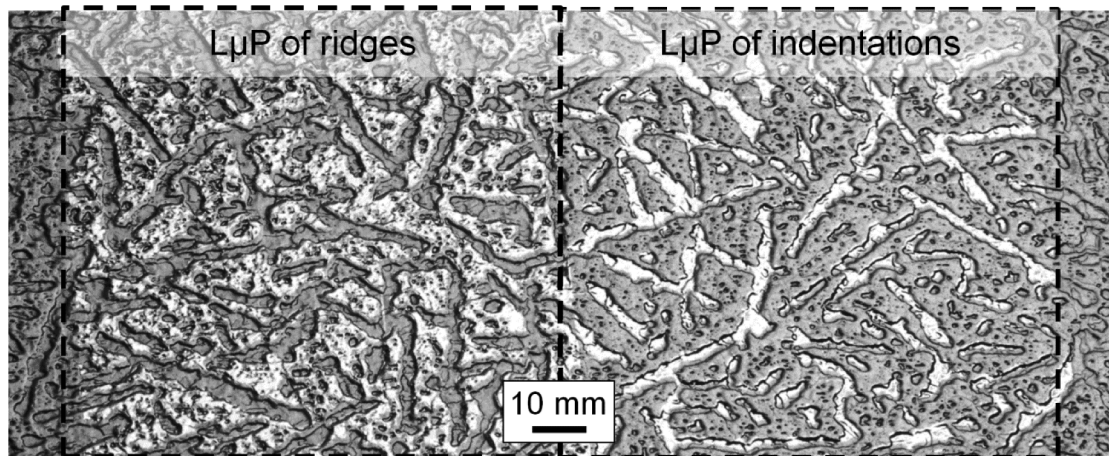


Fig. 27. Example of dual gloss effects on AISI 410 created by selective L μ P of ridges (left) or indentations (right).

by using the data and process chain developed by Temmler et al. [26].

In Fig. 27 a small scale dual gloss effect was created by selective laser polishing of defined parts of the surface structure. On the left side of Fig. 27 the ridges of the surface's structure were selectively laser polished. However, a polishing of only the ridges can also be achieved easily by conventional polishing techniques. A similar effect can be achieved by selectively laser polishing the indentations of the textured surface as shown in Fig. 27(right). A large investment of time and precision would be necessary in order to achieve this effect by means of conventional polishing techniques.

Furthermore, this kind of dual gloss effect can be applied to large scale textured surface like wood grain structures on press plates for decorative laminates Fig. 28. In this case, the indentations of the wood grain structure were polished by L μ P.

In this investigation, process parameters that already lead to a significant reduction of roughness are scanning velocity of $v_{\text{scan}} = 1000 \text{ mm/s}$ at $f_p = 60 \text{ kHz}$ (Fig. 23b) and a track offset of

$dy = 25 \mu\text{m}$. This leads to an area rate of $25 \text{ mm}^2/\text{s}$ or approx. 11 h/m^2 at an average laser power of approx. $P_L = 35 \text{ W}$. This area rate does not seem to be feasible yet for selective L μ P of large areas. However, an upscaling of the area rate should be able to be managed in two steps. Firstly, fiber laser systems are currently available which have a significantly higher average laser power output (100–200 W) at higher maximum pulse frequencies (up to one Megahertz). As shown in this study, by increasing pulse frequency and scanning velocity, the area rate can be significantly increased, which makes for a factor of at least three¹⁵. Secondly, the quantity of laser beam sources can be increased and therefore a parallel processing with multiple laser beams can be achieved. From a technical and economical point of view, four or more laser beam sources seem to be a feasible approach, so that a further

¹⁵Nüsser [2] even demonstrated that area rates of up to 8.8 min/m^2 are possible for laser beams as large as $d_L = 611 \mu\text{m}$ and pulse energies up to $E_p = 25 \text{ mJ}$ for a pulse frequency of $f_p = 20 \text{ kHz}$.

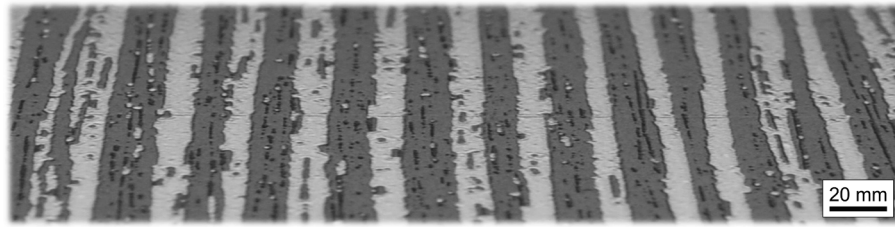


Fig. 28. Example of dual gloss effects on AISI410 created by selective L μ P of indentations.

increase of process speed by a factor of four is easily achievable. Combining both measures would lead to a reduction of the area rate by more than one order of magnitude to approx. 0.5–1 h/m². Area rates of this magnitude are already very well suited for industrial production and might be a crucial stepping-stone to bring L μ P into a wider range of industrial applications.

4. Concluding remarks

The stainless steel AISI 410 and the laser beam source SPI-G3 are well suited for L μ P, since no defects, cracks or scratches have been observed after L μ P. At the same time, a significant reduction in micro-roughness is achieved with all examined waveforms and pulse durations in the range of 10 ns to 220 ns, especially by adapting the fluence and pulse frequency accordingly. The minimum roughness achieved in the micro-roughness regime corresponds to results obtained for other steel materials, which are also very suitable for L μ P (e.g. for tool steel AISI H11). The gloss level of the surface is increased according to the decrease in micro-roughness, as can be seen by visual examination. This makes the material particularly interesting for design applications such as selective laser polishing of press plates for decorative laminates, as can be seen in Fig. 28.

In addition to this overall evaluation, there are further specific results of this study that are of special interest:

- The highest spatial frequency or lowest spatial wavelength is smoothed using the longest pulse duration for otherwise identical process parameters. However, for pulse durations from 10 ns to 130 ns, it was shown that with adaption of pulse frequency, the minimal roughness was no longer dependent on pulse duration.
- The laser polishing fluence F_{pol} becomes smaller for shorter pulse durations. The shorter the pulse duration, the higher the pulse frequency necessary to achieve the maximum reduction of surface roughness. A reduction of the temporal and local PPD leads to an increased heat accumulation, so that overall, a smaller fluence is required for laser polishing. Local heat accumulation enables an effective smoothing of micro roughness at pulse durations of approx. 10 ns, but the required average laser power increases. Significant differences between the minimal achievable roughness for pulse durations in the range of 10 ns to 130 ns could not be identified.
- Spatial and temporal pulse-to-pulse distance (PPD) are of significant importance for L μ P. The choice of the pulse frequency determines the temporal PPD, while the choice of scan speed in combination with pulse frequency determine the spatial PPD. Both lead independently to local heat accumulation that influences both the required laser polishing fluence F_{pol} and the minimum achievable micro roughness. The right choice of laser beam diameter, pulse frequency, and scanning speed is, therefore, of decisive importance
- Indications for a continuous remelting process were observed at high pulse frequencies, although pulsed laser radiation was used. If the cumulative or effective pulse duration ($t_{p,eff} = d_L \cdot v_{scan}^{-1} \cdot t_p$) is in the range of the temporal PPD, a quasi-continuous melting process is assumed to be formed at laser polishing fluence F_{pol} and critical scanning velocity ($v_{scan, crit} < d_L \cdot t_p \cdot f_p^2$). Furthermore, for

this quasi-continuous remelting process, the formation of Marangoni flow is expected to be more likely than in a discrete remelting process.

- Approximately 20 remelting cycles are required for areal processing to achieve a minimal roughness. If the pulse energy is sufficiently high, this can be achieved by adjusting pulse overlap (by scan speed and pulse frequency) and track offset accordingly. As a rule of thumb, pulse overlap and track offset can be the same, and can be about one fifth to one sixth of the laser beam diameter. However, local heat accumulation due to an adequate choice of pulse overlap (scan speed and pulse frequency) is more important than an exact choice of the track offset dy.
- A high pulse-to-pulse stability enables the laser polishing process to be carried out close to the ablation threshold. Formation of unwanted structures due to material ablation or vapor pressure was not observed. The pulse-to-pulse stability for the SPI-G3 fiber laser was measured to be $\pm 2.57\%$ of average pulse energy and helped to achieve homogenous results in surface roughness without cracks or holes.
- An influence of the size of the laser beam diameter on the minimum achievable roughness could not be determined within this investigation. However, a larger laser beam diameter with otherwise identical process parameters leads to an increase in remelting cycles and local heat accumulation. Therefore, both effects should affect the required laser polishing fluence, the resulting surface roughness and the critical spatial frequency.

Finally, from a practical point of view and in addition to these basic findings, the authors also provide a large number of specific process parameters that enable L μ P using a commercially available laser system at different pulse durations, pulse frequencies, scanning velocities, and laser beam diameters. Taking into account currently available fiber lasers, which have an average laser power of more than 100 W, pulse energies in the range of one to five millijoules, pulse frequencies up to the megahertz range, and pulse durations in the three-digit nanosecond range, area rates of several square meters per hour are within the reach for selective and areal L μ P. From a technical and economic point of view, the basic prerequisites for a successful implementation of selective or large-area L μ P in industrial production chains are thus fulfilled.

CRediT authorship contribution statement

A. Temmler: Conceptualization, Methodology, Data curation, Validation, Formal analysis, Investigation, Visualization, Writing - original draft, Writing - review & editing, Supervision. **D. Liu:** Resources, Writing - review & editing. **J. Luo:** Resources, Funding acquisition. **R. Poprawe:** Resources, Funding acquisition.

Declaration of Competing Interest

The authors declare that they have no known competing financial interests or personal relationships that could have appeared to influence the work reported in this paper.

Acknowledgement

The authors thank the German Federal Ministry of Education and Research (BMBF) for the gracious funding of the multilateral collaboration project “MultiSurf - Mikro- und nanoskalige Oberflächenfunktionalisierung durch Multistrahl-Laserverfahren” within the funding initiative “Die Basis der Photonik: Funktionale Oberflächen und Schichten” under grant number 13N13096. The authors also thank the Fraunhofer Institute for Laser technology and RWTH Aachen University for enabling and support of this work. Furthermore, the authors thank the International Joint Research Laboratory of the State Key Laboratory of Tribology at Tsinghua University for their generous support of the project “Laser polishing and structuring by laser remelting”. The results above were acquired partially using facilities and devices funded by the German Federal State of North-Rhine Westphalia within the Center for Nanophotonics under grant number 290047022. Furthermore, this work is supported by the National Natural Science Foundation of China (no. 51527901, 51575298, 51705284, 51705285, and 11890672).

References

- [1] E.V. Bordatchev, A.M.K. Hafiz, O.R. Tutunea-Fatan, *Int. J. Adv. Manuf. Technol.* 73 (2014) 35–52, <https://doi.org/10.1007/s00170-014-5761-3>.
- [2] C. Nüsser, *Lasermikropolieren von Metallen: Laser micro polishing of metals*, 1st ed., Apprimus Verlag, Aachen, 2018 ISBN: 978-3-8635-9618-7.
- [3] E. Willenborg, *Polieren von Werkzeugstählen mit Laserstrahlung*, Zugl.: Aachen, Techn. Hochsch., Diss. (2006), Shaker Verlag, Aachen, 2006, ISBN: 978-3-8322-4896-3.
- [4] A. Temmler, *Selectives Laserpolieren von metallischen Funktions- und Designoberflächen* (engl. Selective laser polishing of functional and design surfaces for metals), Zugl.: Aachen, Techn. Hochsch., Diss. (2013) Shaker Verlag, Aachen, 2013, ISBN: 978-3-8440-1997-1.
- [5] F.E. Pfefferkorn, N.A. Duffie, X. Li, M. Vadali, C. Ma, *CIRP Ann.* 62 (2013) 203–206, <https://doi.org/10.1016/j.cirp.2013.03.112>.
- [6] A. Temmler, K. Graichen, J. Donath, *LTJ* 7 (2010) 53–57, <https://doi.org/10.1002/latj.201090028>.
- [7] R. Ostholt, *Lasermikropolieren metallischer Freiformflächen*, Zugl.: Aachen, Techn. Hochsch., Diss. (2011) Shaker Verlag, Aachen, 2012, ISBN: 978-3-8440-0696-6.
- [8] Flemmer J., *CAM-NC-Datenkette Für Die Laserbearbeitung von Freiformflächen Mit Simultaner Bewegung Mechanischer Achsen Und Galvanometrischem Laserscanner: CAM-NC Data Chain for Laser Processing of Freeform Surfaces with Simultaneous Movement of Mechanical Axes and Galvanometric Laser Scanner*, First ed., Apprimus Verlag, Aachen, 2018 ISBN: 978-3-8635-9644-6.
- [9] T. Kiedrowski, *Oberflächenstrukturbildung beim Laserstrahlpolieren von Stahlwerkstoffen*, Zugl.: Aachen, Techn. Hochsch., Diss. (2009), Shaker Verlag, Aachen, 2009, ISBN: 978-3-8322-874-12.
- [10] T.M. Shao, M. Hua, H.Y. Tam, E.H.M. Cheung, *Surf. Coat. Technol.* 197 (2005) 77–84, <https://doi.org/10.1016/j.surfcoat.2005.01.010>.
- [11] T.L. Perry, *A numerical and experimental study of pulsed laser micro polishing of metals at the meso/micro scale*, PhD Thesis, Madison, Wisconsin, USA (2009) UMI Number: 3368039.
- [12] M.T.C. Chow, A.M.K. Hafiz, O.R. Tutunea-Fatan, G.K. Knopf, E.V. Bordatchev, *Proceedings of the ISOT 2010 International Symposium on Optomechanical Technologies*, Toronto, IEEE, 2010, pp. 1–6, <https://doi.org/10.1109/ISOT.2010.5687316>.
- [13] M. Vadali, C. Ma, N.A. Duffie, X. Li, F.E. Pfefferkorn, in: *Proceedings of the ASME international manufacturing science and engineering conference 2011*, ASME, New York, 2011, pp. 409–417, doi: 10.1115/MSEC2011-50180.
- [14] M. Vadali, C. Ma, N.A. Duffie, X. Li, F.E. Pfefferkorn, *J. Manuf. Processes* 14 (2012) 307–315, <https://doi.org/10.1016/j.jmapro.2012.03.001>.
- [15] M. Vadali, C. Ma, N.A. Duffie, X. Li, F.E. Pfefferkorn, *J. Micro Nano-Manuf.* 1 (2013) 11006, <https://doi.org/10.1115/1.4023756>.
- [16] C. Ma, M. Vadali, N.A. Duffie, F.E. Pfefferkorn, X.C. Li, in: *Proceedings of the 8th International Conference on MicroManufacturing ICOMM 2013*, Northwestern University, Evanston, 2013, Contribution 36, <https://minds.wisconsin.edu/handle/1793/65188>.
- [17] C. Ma, M. Vadali, N.A. Duffie, F.E. Pfefferkorn, X. Li, *J. Manuf. Sci. Eng.* 135 (2013) 61023, <https://doi.org/10.1115/1.4025819>.
- [18] C. Nüsser, J. Kumstel, T. Kiedrowski, A. Diatlov, E. Willenborg, *Adv. Eng. Mater.* 17 (2015) 268–277, <https://doi.org/10.1002/adem.201400426>.
- [19] J. Cho, D.F. Farson, K.J. Hollis, J.O. Milewski, *J. Mech. Sci. Technol.* 29 (2015) 1715–1722, <https://doi.org/10.1007/s12206-015-0344-2>.
- [20] A. Temmler, O. Pütsch, J. Stollenwerk, E. Willenborg, P. Loosen, *Opt. Exp.* 22 (2014) 1387–1393, <https://doi.org/10.1364/OE.22.001387>.
- [21] A. Temmler, D.M. Liu, S. Drinck, J.B. Luo, R. Poprawe, *J. Mater. Process. Technol.* 277 (2020) 116450, <https://doi.org/10.1016/j.jmatprotec.2019.116450>.
- [22] A.M.K. Hafiz, E.V. Bordatchev, R.O. Tutunea-Fatan, *Int. J. Adv. Manuf. Technol.* 70 (2014) 1963–1978, <https://doi.org/10.1007/s00170-013-5408-9>.
- [23] Y.-D. Chen, W.-J. Tsai, S.-H. Liu, J.-B. Horng, *Opt. Laser Technol.* 107 (2018) 180–185, <https://doi.org/10.1016/j.optlastec.2018.05.025>.
- [24] M. Vadali, *Advanced Study of Pulsed Laser Micro Polishing*, PhD Thesis, Madison, Wisconsin, USA, 2013. UMI Number: 3589204.
- [25] J.D. Morrow, *Surface Microstructure and Properties of Pulsed Laser Micro Melted S7 Tool Steel*. PhD. Thesis, Madison, 2015, ProQuest Number: 10168321.
- [26] A. Temmler, E. Willenborg, K. Wissenbach, *Physics Procedia* 12 (2011) 419–430, <https://doi.org/10.1016/j.phpro.2011.03.053>.
- [27] T.A. Mai, G.C. Lim, *J. Laser Appl.* 16 (2004) 221–228, <https://doi.org/10.2351/1.1809637>.
- [28] O. Pütsch, A. Temmler, J. Stollenwerk, E. Willenborg, P. Loosen, in: *F. Dorsch (Ed.), High-Power Laser Materials Processing: Lasers, Beam Delivery, Diagnostics, and Applications IV*, SPIE, 2015, 93560U, doi: 10.1117/12.2076051.
- [29] C. Nüsser, I. Wehrmann, E. Willenborg, *Physics Procedia* 12 (2011) 462–471, <https://doi.org/10.1016/j.phpro.2011.03.057>.
- [30] C. Nüsser, H. Sändker, E. Willenborg, *Physics Procedia* 41 (2013) 346–355, <https://doi.org/10.1016/j.phpro.2013.03.087>.
- [31] R. Poprawe, *Tailored Light 2: Laser Application Technology*/Reinhart Poprawe, Springer, Heidelberg, 2011. ISBN: 978-3-6420-1236-1.
- [32] C.-S. Chang, T.-H. Chen, T.-C. Li, S.-L. Lin, S.-H. Liu, J.-F. Lin, *J. Mater. Process. Technol.* 229 (2016) 22–35, <https://doi.org/10.1016/j.jmatprotec.2015.09.009>.
- [33] C.-S. Chang, C.-K. Chung, J.-F. Lin, *J. Mater. Process. Technol.* 234 (2016) 177–194, <https://doi.org/10.1016/j.jmatprotec.2016.03.024>.
- [34] C.-S. Chang, K.-S. Yang, C.-K. Chung, J.-F. Lin, *Int. J. Adv. Manuf. Technol.* 92 (2017) 1643–1658, <https://doi.org/10.1007/s00170-017-0264-7>.
- [35] A. Temmler, E. Willenborg, K. Wissenbach, in: *G. Hennig, X. Xu, B. Gu, Y. Nakata (Eds.), Laser Applications in Microelectronic and Optoelectronic Manufacturing (LAMOM) XVII*, SPIE, 2012, 82430W, doi: 10.1117/12.906001.
- [36] T.L. Perry, D. Werschmoeller, N.A. Duffie, X. Li, F.E. Pfefferkorn, *J. Manuf. Sci. Eng.* 131 (2009) 21002, <https://doi.org/10.1115/1.3075874>.
- [37] T.L. Perry, D. Werschmoeller, X. Li, F.E. Pfefferkorn, N.A. Duffie, *J. Manuf. Sci. Eng.* 131 (2009) 31002, <https://doi.org/10.1115/1.3106033>.
- [38] F.E. Pfefferkorn, N.A. Duffie, J.D. Morrow, Q. Wang, *CIRP Ann.* 63 (2014) 237–240, <https://doi.org/10.1016/j.cirp.2014.03.055>.
- [39] V.M. Yermachenko, Y.A. Vdovin, V.D. Mironov, N.V. Naumov, V.N. Petrovskiy, N.M. Prokopova, V.I. Polsky, P.S. Dzhumaev, V.L. Yakushin, *Laser Phys.* 20 (2010) 1537–1544, <https://doi.org/10.1134/S1054660X10120042>.
- [40] H. Li, S. Costil, V. Barnier, R. Oltra, O. Heintz, C. Coddet, *Surf. Coat. Technol.* 201 (2006) 1383–1392, <https://doi.org/10.1016/j.surfcoat.2006.02.012>.
- [41] R. Weber, T. Graf, C. Freitag, A. Feuer, T. Kononenko, V.I. Konov, *Opt. Exp.* 25 (2017) 3966–3979, <https://doi.org/10.1364/OE.25.003966>.
- [42] R. Weber, T. Graf, P. Berger, V. Onuseit, M. Wiedenmann, C. Freitag, A. Feuer, *Opt. Exp.* 22 (2014) 11312–11324, <https://doi.org/10.1364/OE.22.011312>.
- [43] J. Preußner, S. Oeser, W. Pfeiffer, A. Temmler, E. Willenborg, *IJMR* 105 (2014) 328–336, <https://doi.org/10.3139/146.111027>.
- [44] C. Liebing, *Beeinflussung funktioneller Oberflächeneigenschaften von Stahlwerkstoffen durch Laserpolieren*, Aachen Techn. Hochsch. Diss. (2010) Aachen, 2010.
- [45] J.D. Morrow, Q. Wang, N.A. Duffie, F.E. Pfefferkorn, https://minds.wisconsin.edu/bitstream/handle/1793/68778/0103_FI.pdf.
- [46] M. Moradi, D. Ghorbani, M.K. Moghadam, M. Kazazi, F. Rouzbahani, S. Karazi, *J. Alloy. Compd.* 795 (2019) 213–222, <https://doi.org/10.1016/j.jallcom.2019.05.016>.
- [47] A. Temmler, E. Willenborg, K. Wissenbach, *U. Mat-wiss, Werkstofftech* 46 (2015) 692–703, doi:10.1002/mawe.201500345.